

*Interactive comment on “Characterization of an EKO MS-711 spectroradiometer: aerosol retrieval from spectral direct irradiance measurements and corrections of the circumsolar radiation” by Rosa Delia García-Cabrera et al.*

**Referee #1: Lionel Doppler**

**GENERAL COMMENTS**

This paper presents a method to retrieve aerosol optical depth (AOD) out of spectral DNI (direct sun normal irradiance) radiation measurements from the spectroradiometer EKO MS-711. The paper presents the instrument, the site of the observations (IZO: Izaña Atmospheric Observatory), and the method used. An issue that is well discussed is how to correct the measured DNI, obtained with the EKO instruments that has a larger field of view than the WMO standards suggest for AOD measurements. The solution found is to estimate the CSR (circumsolar radiation) by simulating the forwarded scattered radiation with a radiative transfer code and multiplying it with a so-called penumbra function depending on the solar angles (azimuth and zenith). The method of AOD inversion is validated thanks to a comparison to a reference instrument (the Cimel – Aeronet photometer) for six wavelengths in UVA, VIS and NIR at the site of IZO during four months (April – July 2019). A statistical study is presented to validate the AOD retrieval method and evaluate the gains of the CSR correction.

The most innovative part of the paper is the presentation of the CSR estimation and the correction of the DNI for this instrument having a field of view of 5° in order to be compared to photometers having a field of view of less than 1.2°(WMO standards). This method is well explained in the paper and the reader can be convinced of the reliability of it.

The main concept presented in the paper is the AOD retrieval out of spectral DNI measurements from a spectroradiometer, this is not new, but only few articles are making a detailed presentation of the method explaining each step and showing all the equations. This is well done in this paper and will be useful for the AOD community, the photometer community and the spectroradiometer community.

The validation of the method is shown thanks to a detailed statistic comparison to a reference instruments, mentioning WMO traceability criteria and discussing objectively, fairly and humbly the weak points of the method and instrument. Thus, substantial conclusions are reached: the paper evaluates quantitatively the DNI correction method, the AOD retrieval method and its application to the instrument EKO MS-711, convincing the readers that these methods can be used operationally with this instrument.

The scientific methods used are well described their validity are discussed, a good balanced use of figures and mathematic equations contributes to a clear outline of them.

The references list is complete enough giving proper credit to current and past work related to this topic. The number of references is good balanced and the references are of excellent quality. Thanks to this literature work, the authors could clearly put forward their own contribution to the topics approached in this paper.

The title of the paper reflects the content of the paper in a good way; the abstract is a good complement of the title and a concise and truth summary of the paper.

The overall presentation is well structured, and despite some minor details (to which I suggested improvements in the part below named "technical comments") clear expressed.

The language is fluent and precise and it is an obstacle neither to get rapidly a good comprehensive view of this work nor to understand the technical and mathematical details. The mathematical formulae are shown in a good way. The equations are correct written, without mistake and well understandable.

I would suggest some minor improvements to be done: A table with all acronyms would be welcome. Also, I join a list of technical corrections (see below: "technical comments"). Moreover, some points should be briefly discussed, these questions are asked below in "specific comments". These are minor/technical corrections that I suggest.

Despite these technical corrections that have to be done, the article is of good scientific quality, of good significance and of good presentation. This justifies my evaluation here above and the fact that I suggest the editor to accept the manuscript and to ask for technical corrections and to answer to the four questions mentioned here below in "specific comments / questions"

*Authors: We appreciate the positive and constructive comments. Below we answer Dr. Doppler's comments.*

## 2. SPECIFIC COMMENTS / QUESTIONS

**C1.- About the CSR correction presented in 3.4.: The simulated forwarded scattering radiation is computed using desert dust aerosol. How can we adapt the correction factors to other type of aerosols? And if it is possible: How is it possible to integrated the characterization of the aerosol kind in an operational algorithm in order to have directly the CSR correction factors suitable to the defined aerosol type?**

*Authors: The correction proposed in this work can be adapted to other types of aerosol- mixtures or sites. We have only used dust since at Izaña Observatory only two very contrasting situations are normally present: clean atmosphere with almost no aerosols, or dusty conditions under Saharan intrusions, mainly in summer. So, the correction factor has been specifically determined for dust aerosol.*

*Any way, we have included in the paper the following information from LibRadtran simulations that can be used for other types of aerosols. Apart from the graph, we have included in the Appendix B, a table with simulated CR values as a function of AOD for different types of aerosols. These values could be used in an operational AOD correction formula.*

*We have added this information in the final manuscript as follows:*

*"...These results have been simulated considering the typical conditions of IZO where mineral dust is practically the only aerosol present (Berjón et al., 2019; García et al., 2017). Simulations of the effect on CR of the eight OPAC mixture aerosols available in LibRadtran model, continental (clean, average and polluted), urban, maritime (clean, polluted and tropical) and desert aerosols (Hess et al., 1998), and for a FOV=5°, are shown in Figure 6. For SZA=30°, with an AOD<sub>500nm</sub> range between 0 and 2 at sea level,*

two defined groups are distinguished: the continental and urban aerosol mixtures, and the maritime and desert dust mixtures. It should be noted that for stations located in urban or continental (clean and contaminated) environments, which are the majority, the correction that would have to be made to the AOD for a very high aerosol load (e.g., AOD = 1) would be much lower, between 1/3 to 1/6, than the correction that would have been performed in the case of dust aerosol. (Figure 6 and Appendix B)."

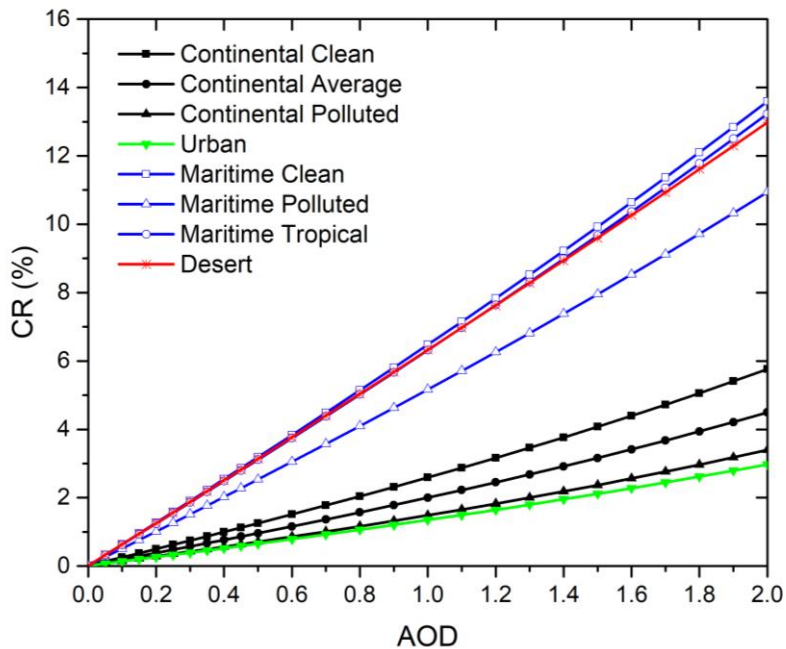


Figure 6. Simulations of CR (%) for SZA 30° at sea level for AOD values between 0 and 2, at 500 nm, for different types of aerosols for FOV of 5°.

The following references have been added:

Berjón, A., Barreto, A., Hernández, Y., Yela, M., Toledano, C., and Cuevas, E.: A 10-year characterization of the Saharan Air Layer lidar ratio in the subtropical North Atlantic, *Atmos. Chem. Phys.*, 19, 6331-6349, <https://doi.org/10.5194/acp-19-6331-2019>, 2019.

García, M. I., Rodríguez, S., and Alastuey, A.: Impact of North America on the aerosol composition in the North Atlantic free troposphere, *Atmos. Chem. Phys.*, 17, 7387-7404, <https://doi.org/10.5194/acp-17-7387-2017>, 2017.

Hess, M., Koepke, P., and Schult, I.: Optical properties of aerosols and clouds: The software package OPAC, *B. Am. Meteorol. Soc.*, 80, 831–844, 1998.

We have added the following table in the Appendix B with the numbers plotted in Figure 6.

(Table of Appendix B) Numerical values of the CR (%) simulations for SZA 30° at sea level for AOD values between 0 and 2, at 500 nm, for different types of aerosols for FOV of 5°.

AOD	Continental Clean CR (%)	Continental Average CR (%)	Continental Polluted CR (%)	Urban CR (%)	Maritime Clean CR (%)	Maritime Polluted CR (%)	Maritime Tropical CR (%)	Desert CR (%)
0.1	0.3	0.2	0.1	0.1	0.6	0.5	0.6	0.6
0.2	0.5	0.4	0.3	0.3	1.3	1.0	1.2	1.3
0.3	0.7	0.6	0.4	0.4	1.9	1.5	1.9	1.9
0.4	1.0	0.8	0.6	0.5	2.5	2.0	2.5	2.5
0.5	1.3	1.0	0.7	0.7	3.2	2.5	3.1	3.1
0.6	1.5	1.2	0.9	0.8	3.8	3.1	3.7	3.8
0.7	1.8	1.4	1.0	0.9	4.5	3.6	4.4	4.4
0.8	2.0	1.6	1.2	1.1	5.1	4.1	5.0	5.0
0.9	2.3	1.8	1.3	1.2	5.8	4.6	5.7	5.7
1	2.6	2.0	1.5	1.3	6.5	5.2	6.3	6.3
1.1	2.9	2.2	1.7	1.5	7.1	5.7	7.0	7.0
1.2	3.2	2.4	1.8	1.6	7.8	6.3	7.6	7.6
1.3	3.5	2.7	2.0	1.8	8.5	6.8	8.3	8.3
1.4	3.8	2.9	2.2	2.0	9.2	7.4	9.0	8.9
1.5	4.1	3.2	2.4	2.1	9.9	8.0	9.7	9.6
1.6	4.4	3.4	2.6	2.3	10.6	8.5	10.4	10.3
1.7	4.7	3.7	2.8	2.4	11.4	9.1	11.1	10.9
1.8	5.1	3.9	3.0	2.6	12.1	9.7	11.8	11.6
1.9	5.4	4.2	3.2	2.8	12.8	10.3	12.5	12.3
2	5.8	4.5	3.4	3.0	13.6	10.9	13.2	13.0

C2.- IZO is a site of low aerosol amount. The results presented in the statistical study to validate the method (part 4.) shows AOD ranging between 0.0 And 0.2 (eg: Figure 9). How many points of comparison do you have for AOD > 0.15? What do you expect it should happen for other sites having larger AOD (continental sites in middle Europe or close-urban areas)?

Authors: Between 83% and 85% of the data correspond to  $AOD \leq 0.15$  for all wavelengths, while for  $AOD > 0.15$  we have between 13% and 15% of the data in the period April-September 2019 at IZO (see Figure 1).

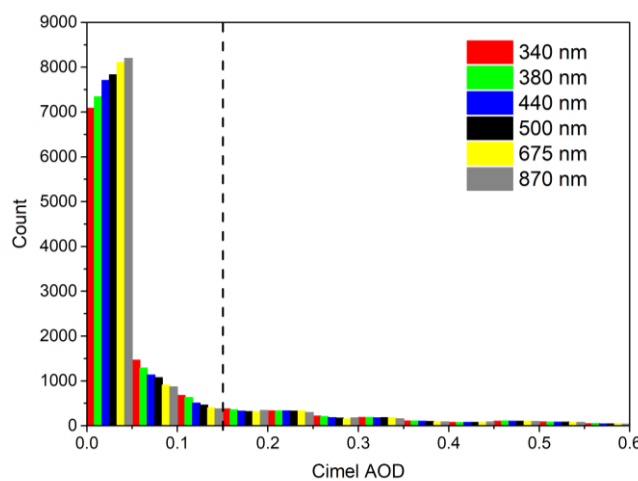


Figure 1.- Frequency of occurrence of Cimel-AOD at all wavelengths between April and September 2019 at IZO.

Considering that our dusty condition threshold value is 0.1, we have added the following information in the final manuscript:

“... The improvement in AOD for AOD>0.1 conditions (**20% of the data for 340 and 380 nm, and 16% for the rest of the wavelengths**) is remarkable, as already mentioned in the CSR correction section. The scatter is also significantly reduced for all wavelengths and aerosol loads...”

According to Figure 6, for continental polluted and urban aerosols the circumsolar radiation is much lower than for dust, so the required AOD corrections should be much lower. The AOD correction for continental pollution and urban aerosols decreases the higher the AOD, faster than makes the correction for dust.

**C3.** Are the results shown in Part 4 restricted to cases with desert dust aerosols? If yes, do you have some preliminary results for other kinds of aerosols? What do you expect it should happen? If no (= the results shown corresponds to different mixtures and kinds of aerosols), do you have some differences between different kinds of aerosols detected?

Authors: Please, see reply to the comment C1

**C4.** The AOD retrieval method presented in 3.1 and 3.2 is well described. Nevertheless, I would discuss two points more in detail: 1) Do you take the same airmass for aerosols, water vapour, mixed gases and ozone? 2) How do you compute Rayleigh optical depth? With which formula (Bodhaine?) and with which values of the air pressure (Aeronet uses a 6 hours average taken from a model)?

Authors:

1) We have not used the same airmass for all the components. We have used the following equations:

- Aerosols and water vapour:  $m_a \approx m_{h2o} = \frac{1}{\cos(\theta) + 0.0548 (92.65 - \theta)^{-1.452}}$  (Kasten, 1966); where  $\theta$  is the solar zenith angle.
- NO<sub>2</sub>:  $m_{NO_2} = \frac{1}{\sin(\theta) + 602.30 (90 - \theta)^{0.5} (27.96 + \theta)^{-3.4536}}$  (Gueymard, 1995)
- Ozone:  $m_{O_3} = \frac{R+h}{\sqrt{(R+h)^2 - (R+r)^2} \sin^2(\theta)}$  (Komhyr, 1989); where  $R$  (6370 km) is the mean radius of the earth,  $r$  is the station height above mean sea level in km, and  $h$  is the mean height of the ozone layer in km (22 km).
- Rayleigh and oxygen:  $m_R \approx m_{O_2} = \frac{1}{\cos(\theta) + 0.50572 (96.07995 - \theta)^{-1.6364}}$  (Kasten and Young, 1989; Gueymard, 2001)

2) The Rayleigh optical depth has been calculated from the following equation:

$\tau_R = \frac{P}{P_0} 0.008569 \lambda^{-4} (1 + 0.0113 \lambda^{-2} + 0.00023 \lambda^{-4})$  (Hansen and Travis, 1974); where  $P$  is the pressure at the measurement site within the earth's atmosphere in KPa,  $P_0$  is the standard pressure at sea level and  $\lambda$  is the wavelength in  $\mu\text{m}$ .

We have used in-situ pressure values used to determine  $\tau_R$  at the same time the spectra were measured..

These equations have been added in the Sect. 3.1 and 3.2 as follow:

### Section 3.1

“...

$$\tau(\lambda) = \tau_R(\lambda) + \tau_a(\lambda) + \tau_{NO_2}(\lambda) + \tau_{H_2O}(\lambda) + \tau_{O_2}(\lambda) + \tau_{O_3}(\lambda) \quad (2)$$

where  $\tau_R(\lambda)$  is the Rayleigh optical depth ([Hansen and Travis, 1974](#)) due to the molecular scattering that depends on the station pressure as well as on the optical air mass ( $m_R$ ) ([Kasten and Young, 1989](#)),  $\tau_a(\lambda)$  is the AOD, and the rest of the terms are the absorption by atmospheric gases in the affected wavelengths ([Gueymard, 2001](#)), which are defined as follows:

$$\tau_R = \frac{P}{P_0} 0.008569 \lambda^{-4} (1 + 0.0113 \lambda^{-2} + 0.00023 \lambda^{-4}) \quad (3)$$

where  $P$  is the pressure at the measurement site within the earth's atmosphere,  $P_0$  is the standard pressure at sea level and  $\lambda$  is the wavelength in  $\mu\text{m}$ . In-situ actual pressure at IZO was used.

$$\tau_{NO_2} = u_{NO_2} A_{NO_2} \quad (4)$$

where  $u_{NO_2}$  is the reduced path-length (in atm-cm) taken from the OMI total column NO<sub>2</sub> monthly average climatology and  $A_{NO_2}$  its spectral absorption coefficient ([Rothman et al., 2013](#)).

$$\tau_{H_2O} = (U_{H_2O} A_{H_2O})^{b_{H2O}} \quad (5)$$

where  $U_{H_2O}$  is the column water vapour content (precipitable water) taken from a Global Navigation Satellite System (GNSS) receiver considering satellite precise orbits at IZO ([Romero Campos et al., 2009](#)),  $A_{H_2O}$  the spectral absorption coefficient [Rothman et al. \(2013\)](#), and the  $b_{H2O}$  exponent depends on the central wavelength position, instrument filter function, as well as the atmospheric pressure and temperature ([Halthore et al., 1997](#)). We have determined  $\tau_{H_2O}$  from the transmittance for different water vapour and solar zenith angle (SZA) values from the MODTRAN model ([Raptis et al., 2018](#)).

$$\tau_{O_2} = (U_{O_2} A_{O_2})^{b_{O2}} \quad (6)$$

where  $U_{O_2}$  is the altitude-dependent gaseous scaled path-length taken from the Fourier transform infrared spectrometer (FTIR) measurements at IZO ([Schneider et al., 2005](#)),  $A_{O_2}$  is the spectral absorption coefficient ([Rothman et al., 2013](#)), and the  $b_{O2}$  exponent was obtained from the transmittance values simulated with the MODTRAN model ([Berk et al., 2000](#)) for IZO, obtaining a value of 0.454. This value is similar to that obtained by [Pierluissi and Tsai \(1986, 1987\)](#).

$$\tau_{O_3} = U_{O_3} A_{O_3} \quad (7)$$

where  $U_{O_3}$  is the total column ozone obtained with a reference Brewer spectrophotometer at IZO ([Redondas et al., 2018](#)), and  $A_{O_3}$  is the ozone absorption cross section ([Brion et al., 1993, 1998](#)).

The Langley-Plot determines  $DNI_o(\lambda)$  (that allows to derive calibration constant) from a linear extrapolation of  $DNI(\lambda)$  measurements to zero air mass, corrected to mean Sun–Earth distance, and plotted on a logarithmic scale versus air mass:

$$\ln(DNI(\lambda)) = \ln DNI_o(\lambda) - [\tau_R(\lambda)m_R + \tau_a(\lambda)m_a + \tau_{NO_2}(\lambda)m_{NO_2} + \tau_{H_2O}(\lambda)m_{H_2O} + \tau_{O_2}(\lambda)m_{O_2} + \tau_{O_3}(\lambda)m_{O_3}] \quad (8)$$

where the different air masses have the following expressions:

$$m_R \approx m_{o2} = \frac{1}{\cos(\theta) + 0.50572 (96.07995 - \theta)^{-1.6364}}; \quad (\text{Kasten and Young, 1989}; \\ \text{Gueymard, 2001}) \quad (9)$$

$$m_a \approx m_{h2o} = \frac{1}{\cos(\theta) + 0.0548 (92.65 - \theta)^{-1.452}}; \quad (\text{Kasten, 1966}) \quad (10)$$

$$m_{NO2} = \frac{1}{\sin(\theta) + 602.30 (90 - \theta)^{0.5} (27.96 + \theta)^{-3.4536}}; \quad (\text{Gueymard, 1995}) \quad (11)$$

$$m_{o3} = \frac{R+h}{\sqrt{(R+h)^2 - (R+r)^2 \sin^2(\theta)}}; \quad (\text{Komhyr, 1989}) \quad (12)$$

where  $R$  (6370 km) is the mean radius of the Earth,  $r$  is the station height above mean see level in km, and  $h$  is the mean height of the ozone layer in km (22 km).

..."

### Section 3.2

"..."

The AOD retrievals have been calculated from Eq. 8, as follows:

$$AOD = \frac{1}{m_a} [\ln DNI_o(\lambda) - \ln DNI(\lambda) - \tau_R(\lambda)m_R - \tau_a(\lambda)m_a - \tau_{NO_2}(\lambda)m_{NO_2} - \tau_{H_2O}(\lambda)m_{H_2O} - \tau_{O_3}(\lambda)m_{O_3}] \quad (14)$$

Grouping the gases contributions as  $\tau_{gas}$ , the AOD expression is reduced to:

$$AOD = \frac{1}{m_a} [\ln DNI_o(\lambda) - \ln DNI(\lambda) - \tau_R m_R - \tau_{gas} m_{gas}] \quad (10)$$

..."

### 3. TECHNICAL COMMENTS

**General comment:** Please introduce a list of all acronyms used

Authors: We have included all acronyms used in the manuscript in Appendix A.

**Abstract:**

- At the beginning of the abstract, should be explained what is the spectral range and resolution of EKO MS-711.

Authors: We have included the spectral range of the spectroradiometer in the abstract as follows:

"Spectral direct UV-Visible normal solar irradiance (DNI) has been measured with an EKO MS-711 grating spectroradiometer, which has a spectral range of 300-1100 nm, 0.4 nm step, at the Izaña Atmospheric Observatory (IZO, Spain) ... "

### Introduction

- L25: "properties, such as single scattering albedo, size distribution, etc" -> please avoid "etc", write a complete list, best sorted in decreasing importance order.

Authors: We have completed this sentence as follows:

*"... therefore it is necessary to make more efforts to evaluate the aerosol atmospheric content and optical properties, such as the aerosol optical depth (AOD), Angström exponent (AE), single scattering albedo (SSA), scattering coefficient, and absorption coefficient."*

- L47: (again etc.) -> please complete list or use "e.g.:"

Authors: We have modified this sentence as follows:

*"... possibility to provide other atmospheric components (e.g., O<sub>3</sub>, NO<sub>2</sub>, SO<sub>2</sub>, CH<sub>4</sub>, and H<sub>2</sub>O)..."*

- L47: reference is Barreto 2014 (and not 2013) for spectroradiometer and Aerosol.

Authors: You are right. The reference will be replaced by Barreto et al. (2014) in the final manuscript.

- L67: Go to next line before presenting the parts of your papers with "We have devided:"

Authors: Done

## Part 2: Site Description, Instrument and ancillary information

2.2 Instrument: Maybe explain what kind of technology it is: monochromator or array spectrometer (it is not specified).

Authors: We have added the instrument type as follows:

*"... An EKO MS-711 grating spectroradiometer used in direct-sun measurement mode has been tested..."*

- L98: Specify in this part of the text that the world AOD reference is the PFR in order that the reader knows from which instrument you are talking about.

Authors: We have addressed this issue as follows:

*"...The different Cimel references have been shown to have a good AOD traceability with the GAW-PFR worldwide reference (Cuevas et al., 2019)..."*

- L104: Bias < 0.01 (and not > 0.01) (citing Sinyuk, GRL 2012)

Authors: Done, it was a typo.

## Part 3. Methodology

- L130+L136+L141, maybe use a different description for "b" of each gas: b\_H<sub>2</sub>O, b\_O<sub>2</sub>, b\_O<sub>3</sub> for example. Here you have the same letter and the reader can think that we have the same coefficient for all the three gases.

Authors: Done in the final manuscript (see question 4: SPECIFICT COMMENT / QUESTIONS)

- L141: What about b\_O3?

Authors: It has been corrected in the manuscript final (see reply to comment C4)

- L167: “dependence [in] particle size”(not [pn])

Authors: Done. It was a typo.

- L167: I cannot understand the whole sentence. Do you mean: “high dependence in particle size [distribution] THROW the aerosol phase function?

Authors: We have clarified this sentence as follows:

“... This CSR has a high dependence on the particle size (Räisänen and Lindfors, 2019), thus large particles (such as desert dust) produce a higher scattering on the incident beam than the smaller particles (e.g., rural background aerosols), leading this contribution to overestimate the DNI...”

- Figure 4.: In the legend, maybe mention that P has no unit and also mention that P\*L (figure on the right) is in W.m-2.sr-1 (like L). If not, the reader has to guess it from L-graphic and P-graphic.

Authors: We have added the units in the legend as follows:

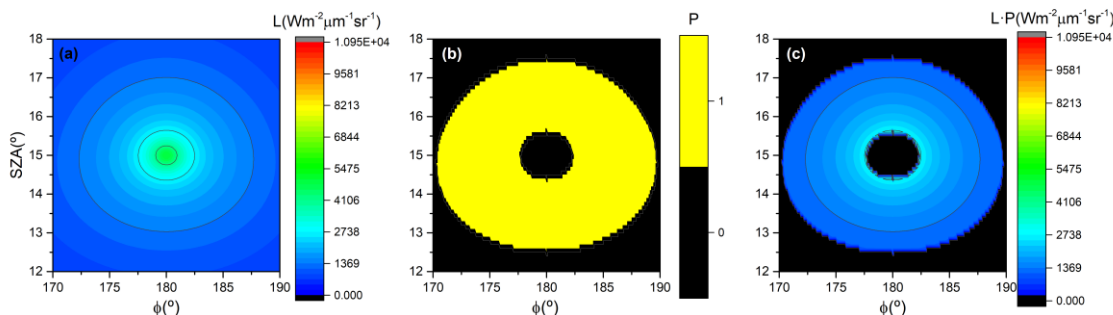


**Figure 4.** Example of the (a) diffuse radiance  $L$  ( $\text{Wm}^{-2}\mu\text{m}^{-2}\text{sr}^{-2}$ ) at 500 nm, shown in colours for different SZA and  $\phi$ ; (b) penumbra function  $P$  determined from Eq. 11 and (c) the product of the diffuse radiance  $L$  and penumbra function  $P$ .

- L231 (Equation 13): Are you sure? I would write:  $\text{DNI}_{\text{corr}} = \text{DNI}_{\text{measured}} - \text{CSR} = \text{DNI}_{\text{SUN}}_{\text{estimation}}$

Authors: You are right, the equation has been modified in the final manuscript as follows:

$$\text{DNI}_{\text{CORR}} = \text{DNI} - \text{CSR}$$

- L239 You define the CR (Circumsolar Ratio). Please write the equation that defines it as Equation 15

Authors: The equation that defines CR has been added in the final manuscript as follows:

$$\text{CR}(\%) = \frac{\text{CSR}}{\text{DNI}_{\text{SUN}} + \text{CSR}} \cdot 100$$

- L248 You cite Equation 15 that does not exist (surely it was your intention that Eq 15 is the definition of CR but you forgot it)

Authors: You are right. We forgot it.

- Figure 7 (Legend): “at at”

Authors: Done

- Table 4: It is unclear regarding the table, which columns are with and which columns are without CSR correction, since it is written “CSR Unc.” everywhere. I guess that in each column pair, left is without and right is with correction, but please correct the header.

Authors: Done, the table has been corrected as follows:

Wavelength (nm)	R		Slope		RMS		MB	
	CSR Unc.	CSR Corr.	CSR Unc.	CSR Corr.	CSR Unc.	CSR Corr.	CSR Unc.	CSR Corr.
340 nm	0.960	0.973	1.063	0.994	0.017 (28.9%)	0.007 (16.9%)	0.015 (24.5%)	<0.001 (-1.4%)
380 nm	0.981	0.986	1.071	1.001	0.009 (20.2%)	0.005 (12.9%)	0.007 (14.8%)	<0.001 (1.2%)
UV-Range	0.971	0.979	1.067	0.997	0.013 (24.6%)	0.006 (14.9%)	0.011 (19.7%)	<0.001 (1.3%)
440 nm	0.984	0.987	1.041	0.997	0.101 (22.4%)	0.005 (13.5%)	0.009 (18.7%)	0.001 (0.6%)
500 nm	0.988	0.991	1.075	1.018	0.007 (18.2%)	0.005 (12.9%)	0.004 (12.1%)	0.002 (0.4%)
675 nm	0.989	0.991	1.057	1.013	0.006 (19.7%)	0.006 (10.7%)	0.003 (11.2%)	<0.001 (0.5%)
870 nm	0.998	0.999	1.039	1.009	0.004 (18.8%)	0.003 (7.3%)	<0.001 (0.3%)	<0.001 (0.2%)
VIS-Range	0.989	0.992	1.053	1.009	0.029 (19.5%)	0.005 (11.1%)	0.004 (10.6%)	<0.001 (0.4%)

**Table 4.** Statistics of the comparison between EKO AOD, with no CSR corrections (CSR Unc.) and implementing CSR corrections (CSR Corr.), and Cimel AOD at 340, 380, 440, 500, 675 and 870 nm at IZO between April and September 2019. R: correlation coefficient, slope of the least-squares fit between EKO AOD and Cimel AOD, RMS: root mean square of the bias and MB: mean bias. The results of the relative bias are in brackets (in %).

- L271 “good agreement”, maybe you should here define what you consider being a “good agreement”, by mentioning WMO traceability criteria that is cited below (L304).

Authors: In this case we are just comparing the AOD provided by the EKO and Cimel. Later, we compare the AOD of both instruments using the WMO traceability criteria. We have clarified what means “good agreement” by adding the correlation coefficient. This sentence reads now as follows:

“... The results show (Table 4) that there is a good agreement (correlation coefficient > 0.98) between EKO AOD and Cimel AOD for all channels, even for no CSR correction...”

- L290 340 nm. Instrumental uncertainty only? Maybe also because Rayleigh is higher and also aerosol scattering is higher -> Same comment for discussion in L311-L312

Authors: The authors have attributed most of the found differences to the instrument uncertainty because the instrument error in the spectral range between 300 and 350 nm is 17.2%, of which 6% corresponds to stray-light, and 6% corresponds to measurement repeatability. Moreover, it is also affected by the different FWHM between EKO (7 nm) and CIMEL (2 nm) at 340 nm, and by the fact that Rayleigh and aerosol scattering are higher in the UV range (Cuevas et al., 2018).

We have added this information in the final manuscript as follows:

“... The scatter also is significantly reduced for all wavelengths and aerosol loads, except in the 340 nm UV channel. This is mainly attributed to the instrumental error in the spectral range between 300 and 350 nm (17.2%), of which 6% corresponds to stray-light and 6% corresponds to measurement repeatability (Zong et al., 2006), to the different FWHM between EKO (7 nm) and CIMEL (2 nm) at 340 nm, and to the fact that Rayleigh and aerosol scattering are higher in the UV range (Cuevas et al., 2019)...”

L291: “model characterization [in] this range”

Authors: Done

- L298: “ $MB \geq -1.6\%$ ” this is confusing, please discuss in absolute: “ $abs(MB) \leq 1.6\%$ ”

Authors: Done

#### References:

For WMO Reports, please cite the page, at least the part of these very large reports in which the information is, in order to help the reader to find the relevant information for this study.

Authors: We have added this information in the final manuscript.

- L570 (Reference WMO, 1986): “GAW Report-No. 43” (not “437”).

Authors: Done

***Interactive comment on “Characterization of an EKO MS-711 spectroradiometer: aerosol retrieval from spectral direct irradiance measurements and corrections of the circumsolar radiation” by Rosa Delia García-Cabrera et al.***

**Referee #2**

The current work presents AOD retrievals from EKO MS-711, compared with CIMEL retrievals at Izaña Observatory and most importantly proposes an approach to correct DNI in respect to different FOV of the instruments using CSR. The paper fits perfectly the purposes of AMT and the proposed correction could find greater use in a number of instruments. Details of the approach are well presented and described sufficient in order to be repeatable. Results presented fortify the validity of the approach and are a guide for future studies of other spectroradiometers. The structure of the presentation is very steady and bibliographical review of the subject is more than sufficient. I suggest the acceptance of the article for publication at AMT, after some minor corrections and clarifications.

Authors: We acknowledge the referee's positive and constructive comments. Below we respond to his/her general comments.

***General Comments:***

**More specifically**

L22. This sentence seems a little poor and inadequate. I suggest to restate.

Authors: We have modified the sentence as follows:

*“One of the most important elements that governs the Earth’s climate, and its processes, is the presence of atmospheric aerosols, which produce a significant radiative forcing resulting from light scattering and absorption, and radiation emission. Moreover, they act as cloud condensation nuclei, modifying cloud properties (IPCC, 2013). Aerosols effect on the Earth Radiation Balance has been quantified as a cooling of  $-0.45 \text{ W m}^{-2}$ , and  $-0.9 \text{ W m}^{-2}$  when considering the combined effect of both aerosols and clouds...”*

Paragraph 2.2 1) I think some information on the measuring schedule should be added. 2) There is one spectral per minute or they are multiple spectra averaged and stored per minute? 3) Exposure time is steady or it is changed according to the intensity of the irradiance? 4) Are there oversaturation problems? 5) Are there any filters used?

Authors:

1) and 2) The EKO MS-711 spectroradiometer measures one spectrum per minute.

3) The exposure time is not constant. The setting changes automatically according to the intensity of the irradiance, and varies from 10 ms to 5 s.

4) As a result of the optimized exposure time for the irradiance and the instrument measurement dynamic range, no saturated measurements are experienced.

5) This instrument does not use filters.

Followings the recommendations of the referee, we have added this information as follows:

## Section 2.2

*"An EKO MS-711 grating spectroradiometer used in direct sun measurement mode has been tested (Figure 1) within the CIMO Testbed program from April to September 2019 (14706 datapoints)..."*

*"...This spectroradiometer has been mounted on an EKO sun-tracker STR-21G-S2 (accuracy of <0.01°). This setup performs one spectrum per minute, with an exposure time that changes automatically according to the intensity of the irradiance that varies from 10 ms to 5 s. The main specifications of the EKO MS-711 spectroradiometer are shown in Table 1..."*

**L105** Level 1.5 are automatic cloud screening and the quality assured data are **L2.0**. Please restate to be clear.

Authors: The authors have not used Level 2.0 because it is not available for the study period (April and September 2019) in AERONET. We have modified the sentence as follows:

*"...In this study, we have used AERONET Version 3.0 Level 1.5 AOD data..."*

**L155** Have you used O3 in the calculations? There is nothing about it and at least for 340nm is important. If you have not calculated ozone absorption probably it could explain a part of the differences at 340 nm.

Authors: Yes. We have taken into account ozone column in the AOD retrievals at 340, 500 and 675 nm (see Table 2 of the manuscript). The ozone values used have been measured with a reference double Brewer spectroradiometer at Izaña station, therefore it does not explain the differences found at 340 nm.

This information is given in the Section 3.1, however, the authors have added this information in the Section 3.2 as follows:

*"...In this work, we have calculated the EKO AOD at the same nominal wavelengths as those of the Cimel (340, 380, 440, 500, 675 and 870 nm) following the methodology used by AERONET (Holben et al. (2001); Giles et al. (2019), and references herein). For each wavelength, we have taken into account the spectral corrections shown in Table 2. All wavelengths have been corrected by the Rayleigh scattering (see Sect. 3.1). Furthermore the 340, 380, 440 and 500 nm are corrected from nitrogen dioxide (NO<sub>2</sub>) absorption, being the optical depth calculated using the OMI total column NO<sub>2</sub> climatological monthly averages, and the NO<sub>2</sub> absorption coefficient from Burrows et al. (1999). The 340, 500 and 675 nm channels are corrected of ozone, using the ozone values from the Izaña WMO-GAW reference Brewer spectroradiometer..."*

**L166-167** Please restate this sentence because it is not clear.

Authors: We have modified the sentence as follows:

“... This CSR has a high dependence on the particle size (Räisänen and Lindfors, 2019), thus large particles (such as desert dust) produce a higher scattering on the incident beam than the smaller particles (e.g., rural background aerosols), leading this contribution to overestimate the DNI...”

**Paragraph 3.2** The measured spectrum has a resolution of 0.4nm with FWHM of 7 nm. When referring to monochromatic retrievals of AOD, have you used just one channel(which?) or do you have convoluted multiple channels to a slit function? Please clarify this because it is crucial for understanding the differences with AERONET. For example lines 293-295 confused me on this matter. Also, I think it should be cleared if there any other difference with AERONET calculations (air masses, Rayleigh etc).

Authors: For determining the AOD with the EKO MS-711 spectroradiometer, we have considered the same nominal wavelengths and bandwidths (Filter Bandpass) as those of the Cimel (340: 2 nm, 380: 4 nm, 440: 5 nm, 500: 5 nm, 675: 5 nm and 870: 5 nm) as indicated on Table 2 of the manuscript. Centred on each wavelength and with its corresponding bandwidth, we have performed the integration of the irradiance on the considered spectral range. For example, in the AOD retrieval at 500 nm, the range 495-505 nm is used to perform the integration:

$$DNI(\lambda) = \int_{495 \text{ nm}}^{505 \text{ nm}} DNI(\lambda)_{EKO-MS711} d\lambda$$

This integrated value is the one used in equations of paragraph 3.2.

We have modified this paragraph as follows:

“...In this work, we have calculated the EKO AOD at the same nominal wavelengths as those of the Cimel (340, 380, 440, 500, 675 and 870 nm), by integrating the measured irradiance on the considered bandpass (see Table 2), following the methodology used by AERONET (Holben et al. (2001); Giles et al. (2019), and references herein). For each wavelength, we have taken into account the spectral corrections shown in Table 2. All wavelengths have been corrected by the Rayleigh scattering (see Sect. 3.1). Furthermore the 340, 380, 440 and 500 nm channels have been corrected from nitrogen dioxide (NO<sub>2</sub>) absorption, being its optical depth calculated using the OMI total column NO<sub>2</sub> climatological monthly averages, and the NO<sub>2</sub> absorption coefficient from Burrows et al. (1999). The 340, 500 and 675 nm channels have been corrected of ozone, using the ozone values from a GAW reference Brewer spectroradiometer sited at Izaña Observatory...”

Regarding the Lines 293-295, maybe the confusion arises in the sentence “some additional radiation contribution from the adjacent wavelengths”. The considered range on each channel are those explained before and, in the paragraph, we tried to highlight that for the UV channels the contribution of the stray-light is important, therefore we have modified the paragraph as follows:

“...Since the 340 nm and 380 nm channels have 2 nm and 4 nm bandpass, respectively, and the EKO MS-711 FWHM is 7nm (Table 1), these two UV channels have some additional radiation contribution from the adjacent wavelengths due to stray-light, increasing their uncertainty and causing an AOD overestimation...”

The equations of air masses and optical depths used are the same to those used by AERONET, and they have been included in the final manuscript.

#### L248 There is no equation 15 in the manuscript

Authors: Thank you. The equation of the CR has been added in the final manuscript as follows:

$$CR(\%) = \frac{CSR}{DNI_{SUN} + CSR} \cdot 100$$

Paragraph 3.4 I understand that dust aerosols are the main in Izaña, but I think it is important to add some discussion of potential differences for other aerosol types.

Authors: We have only used dust since at Izaña Observatory only two very contrasting situations are normally present: clean atmosphere with almost no aerosols, or dusty conditions under Saharan intrusions, mainly in summer. So, the correction factor has been specifically determined for dust aerosol.

Any way, we have included in the paper the following information from LibRadtran simulations that can be used for other types of aerosols. Apart from the graph, we have included in the Appendix B, a table with simulated CR values as a function of AOD for different types of aerosols.

We have added this information in the final manuscript as follows:

*“... These results have been simulated considering the typical conditions of IZO where mineral dust is practically the only aerosol present (Berjón et al., 2019; García et al., 2017). Simulations of the effect on CR of the eight OPAC mixture aerosols available in LibRadtran model, continental (clean, average and polluted), urban, maritime (clean, polluted and tropical) and desert aerosols (Hess et al., 1998), and for a FOV=5°, are shown in Figure 6. For SZA=30°, with an AOD<sub>500nm</sub> range between 0 and 2 at sea level, two defined groups are distinguished: the continental and urban aerosol mixtures, and the maritime and desert dust mixtures. It should be noted that for stations located in urban or continental (clean and contaminated) environments, which are the majority, the correction that would have to be made to the AOD for a very high aerosol load (e.g., AOD = 1) would be much lower, between 1/3 to 1/6, than the correction that would have been performed in the case of dust aerosol. (Figure 6 and Appendix B) ...”*

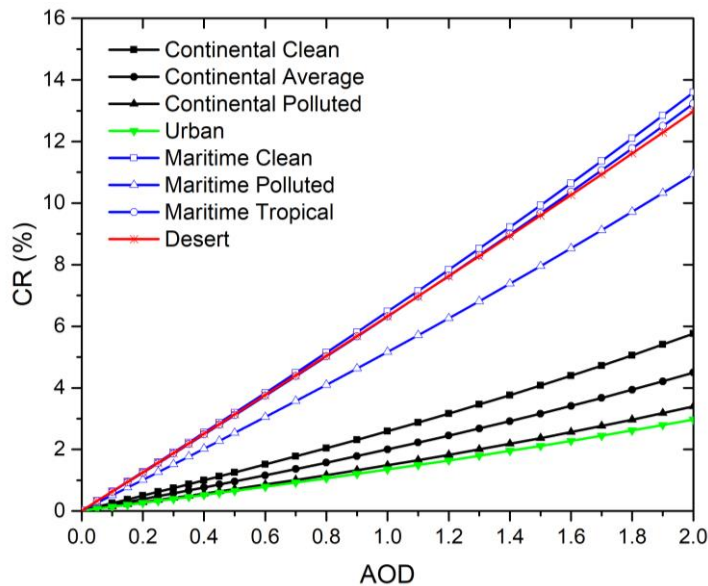


**Figure 6. Simulations of CR (%) for SZA 30° at sea level for AOD values between 0 and 2, at 500 nm, for different types of aerosols for FOV of 5°.**

The following references have been added:

Berjón, A., Barreto, A., Hernández, Y., Yela, M., Toledano, C., and Cuevas, E.: A 10-year characterization of the Saharan Air Layer lidar ratio in the subtropical North Atlantic, *Atmos. Chem. Phys.*, 19, 6331-6349, <https://doi.org/10.5194/acp-19-6331-2019>, 2019.

García, M. I., Rodríguez, S., and Alastuey, A.: Impact of North America on the aerosol composition in the North Atlantic free troposphere, *Atmos. Chem. Phys.*, 17, 7387-7404, <https://doi.org/10.5194/acp-17-7387-2017>, 2017.

Hess, M., Koepke, P., and Schult, I.: Optical properties of aerosols and clouds: The software package OPAC, *B. Am. Meteorol. Soc.*, 80, 831–844, 1998.

We have added the following table in the Appendix B with the numbers plotted in Figure 6.

(Table of Appendix B) Numerical values of the CR (%) simulations for SZA 30° at sea level for AOD values between 0 and 2, at 500 nm, for different types of aerosols for FOV of 5°.

AOD	Continental Clean CR (%)	Continental Average CR (%)	Continental Polluted CR (%)	Urban CR (%)	Maritime Clean CR (%)	Maritime Polluted CR (%)	Maritime Tropical CR (%)	Desert CR (%)
0.1	0.3	0.2	0.1	0.1	0.6	0.5	0.6	0.6
0.2	0.5	0.4	0.3	0.3	1.3	1.0	1.2	1.3
0.3	0.7	0.6	0.4	0.4	1.9	1.5	1.9	1.9
0.4	1.0	0.8	0.6	0.5	2.5	2.0	2.5	2.5
0.5	1.3	1.0	0.7	0.7	3.2	2.5	3.1	3.1
0.6	1.5	1.2	0.9	0.8	3.8	3.1	3.7	3.8
0.7	1.8	1.4	1.0	0.9	4.5	3.6	4.4	4.4
0.8	2.0	1.6	1.2	1.1	5.1	4.1	5.0	5.0
0.9	2.3	1.8	1.3	1.2	5.8	4.6	5.7	5.7

1	2.6	2.0	1.5	1.3	6.5	5.2	6.3	6.3
1.1	2.9	2.2	1.7	1.5	7.1	5.7	7.0	7.0
1.2	3.2	2.4	1.8	1.6	7.8	6.3	7.6	7.6
1.3	3.5	2.7	2.0	1.8	8.5	6.8	8.3	8.3
1.4	3.8	2.9	2.2	2.0	9.2	7.4	9.0	8.9
1.5	4.1	3.2	2.4	2.1	9.9	8.0	9.7	9.6
1.6	4.4	3.4	2.6	2.3	10.6	8.5	10.4	10.3
1.7	4.7	3.7	2.8	2.4	11.4	9.1	11.1	10.9
1.8	5.1	3.9	3.0	2.6	12.1	9.7	11.8	11.6
1.9	5.4	4.2	3.2	2.8	12.8	10.3	12.5	12.3
2	5.8	4.5	3.4	3.0	13.6	10.9	13.2	13.0

**Table 4.** There is typo and all columns seem to be uncorrected.

Authors: Done. The final table is the following:

Wavelength (nm)	R		Slope		RMS		MB	
	CSR Unc.	CSR Corr.	CSR Unc.	CSR Corr.	CSR Unc.	CSR Corr.	CSR Unc.	CSR Corr.
340 nm	0.960	0.973	1.063	0.994	0.017 (28.9%)	0.007 (16.9%)	0.015 (24.5%)	<0.001 (-1.4%)
380 nm	0.981	0.986	1.071	1.001	0.009 (20.2%)	0.005 (12.9%)	0.007 (14.8%)	<0.001 (1.2%)
UV-Range	0.971	0.979	1.067	0.997	0.013 (24.6%)	0.006 (14.9%)	0.011 (19.7%)	<0.001 (1.3%)
440 nm	0.984	0.987	1.041	0.997	0.101 (22.4%)	0.005 (13.5%)	0.009 (18.7%)	0.001 (0.6%)
500 nm	0.988	0.991	1.075	1.018	0.007 (18.2%)	0.005 (12.9%)	0.004 (12.1%)	0.002 (0.4%)
675 nm	0.989	0.991	1.057	1.013	0.006 (19.7%)	0.006 (10.7%)	0.003 (11.2%)	<0.001 (0.5%)
870 nm	0.998	0.999	1.039	1.009	0.004 (18.8%)	0.003 (7.3%)	<0.001 (0.3%)	<0.001 (0.2%)
VIS-Range	0.989	0.992	1.053	1.009	0.029 (19.5%)	0.005 (11.1%)	0.004 (10.6%)	<0.001 (0.4%)

**Table 4.** Statistics of the comparison between EKO AOD, with no CSR corrections (CSR Unc.) and implementing CSR corrections (CSR Corr.), and Cimel AOD at 340, 380, 440, 500, 675 and 870 nm at IZO between April and September 2019. R: correlation coefficient, slope of the least-squares fit between EKO AOD and Cimel AOD, RMS: root mean square of the bias and MB: mean bias. The results of the relative bias are in brackets (in %).

L296-298. Please refer the number of datapoints used for each of the two periods.

Authors: We have added the number of datapoints used for each of the two periods as follows:

“... The linear AOD-correction equations were determined by using data measured from April 1<sup>st</sup> to July 31<sup>th</sup> 2019 (**69% of the data**) at Izaña Observatory (Table 5). The validation of these linear AOD-correction equations was performed using an independent period of data (between August 1<sup>st</sup> and September 30<sup>th</sup> 2019) (**31% of the data**)...”

**L.3131 Also refer the number of data with AOD>0.1**

Authors: *We have added the number of AOD>0.1 as follows:*

*"When focusing the analysis on relatively high AOD (AOD> 0.10), we found that the percentage of AOD differences out of the WMO U<sub>95</sub> limits were ≈ 3.5% (**0.8% of the data**) at 380 nm and 0.6% (**0.3% of the data**) at 870 nm..."*

***Interactive comment on “Characterization of an EKO MS-711 spectroradiometer: aerosol retrieval from spectral direct irradiance measurements and corrections of the circumsolar radiation” by Rosa Delia García-Cabrera et al.***

**Referee #3**

The paper presents results of direct sun measurements and aerosol optical depth (AOD) retrieval for an EKO MS-711 spectroradiometer. An extended investigation is presented for the circumsolar radiation correction.

In my opinion the paper is very well written and is well within the scope of AMT. Spectroradiometers have been used less nowadays for atmospheric monitoring due to reasons that the authors quote in their manuscript and I personally agree. However, they are very important instrumentation as the spectral characteristics of the solar irradiance is the desired one in order to be used for a number of atmospheric-radiation related issues.

I only have some minor comments on the manuscript.

*Authors:* We appreciate the positive and constructive comments of the Referee. Below we respond to his/her general comments.

**Instrument characterization and performance.**

The authors use the term instrument characterization in the title so I would expect some results on other aspects such as linearity, stray light etc.

*Authors:* We fully agree. We have modified the title of the manuscript as follows:

**Title: “Aerosol retrievals from the EKO MS-711 spectral direct irradiance measurements and corrections of the circumsolar radiation”**

In their instruments characteristics table they quote that the instrument step is way less ( $\approx 20$  times) than the optical resolution. Can you provide some more information on how each measurement is performed? is it some kind of averaging? or just a very wide entrance slit?

*Authors:* The EKO MS-711 spectroradiometer measures one spectrum per minute. The exposure time is not constant, but the setting changes automatically the exposure time between 10 ms to 5 s, according to the intensity of the irradiance.

So, we have added this information as follows:

**Section 2.2**

***“...This spectroradiometer has been mounted on an EKO sun-tracker STR-21G-S2 (accuracy of  $<0.01^\circ$ ). This setup performs one spectrum per minute, with an exposure time that changes automatically according to the intensity of the irradiance that varies***

*from 10 ms to 5 s. The main specifications of the EKO MS-711 spectroradiometer are shown in Table 1..."*

**The fact that the optical resolution is  $\approx 7\text{nm}$  compared with  $2\text{nm}$  and  $4\text{nm}$  for CIMEL UV bands (I had the impression that CIMEL 380nm filters are also  $2\text{ nm}$  wide), could be a source of uncertainties in the Rayleigh or Langley constants parameters of the EKO compared with the CIMEL? Meaning that the spectrum relative changes for different solar angles and atmospheric conditions can be different for irradiances at  $340\text{nm} \pm 7\text{nm}$  and  $340\text{nm} \pm 2\text{nm}$ .**

Authors: *For determining the AOD with the EKO MS-711 spectroradiometer, we have considered the same nominal wavelengths and bandwidths (Filter Bandpass) as those of the Cimel (340: 2 nm, 380: 4 nm, 440: 5 nm, 500: 5 nm, 675: 5 nm and 870: 5 nm) as indicated on Table 2 of the manuscript. Centred on each wavelength and with its corresponding bandwidth, we have performed the integration of the irradiance on the considered spectral range. For example, in the AOD retrieval at 500 nm, the range 495-505 nm is used to perform the integration:*

$$DNI(\lambda) = \int_{495 \text{ nm}}^{505 \text{ nm}} DNI(\lambda)_{EKO-MS711} d\lambda$$

*This integrated value is the one used in equations of paragraph 3.2.*

*We have modified this paragraph as follows:*

*"...In this work, we have calculated the EKO AOD at the same nominal wavelengths as those of the Cimel (340, 380, 440, 500, 675 and 870 nm), by integrating the measured irradiance on the considered bandpass (see Table 2), following the methodology used by AERONET (Holben et al. (2001); Giles et al. (2019), and references herein). For each wavelength, we have taken into account the spectral corrections shown in Table 2. All wavelengths have been corrected by the Rayleigh scattering (see Sect. 3.1). Furthermore the 340, 380, 440 and 500 nm channels have been corrected from nitrogen dioxide ( $\text{NO}_2$ ) absorption, being its optical depth calculated using the OMI total column  $\text{NO}_2$  climatological monthly averages, and the  $\text{NO}_2$  absorption coefficient from Burrows et al. (1999). The 340, 500 and 675 nm channels have been corrected of ozone, using the ozone values from a GAW reference Brewer spectroradiometer sited at Izaña Observatory..."*

**The calibration constants and difference with the manufacturer ones seems noisy in the UV range, authors claim that "differences are attributed to the low halogen lamp signal in this region experienced during the factory calibration, and low instrument sensitivity in this region" could this affect AOD at UV results?**

Authors: *Yes, it affects to AOD uncertainty in the UV range. We have clarified this issue as follows:*

*"... The scatter also is significantly reduced for all wavelengths and aerosol loads, except in the 340 nm UV channel. This is mainly attributed to the instrumental error in the spectral range between 300 and 350 nm (17.2%), of which 6% corresponds to stray-light and 6% corresponds to measurement repeatability (Zong et al., 2006), to the different FWHM between EKO (7 nm) and CIMEL (2 nm) at 340 nm, and to the fact that Rayleigh and aerosol scattering are higher in the UV range (Cuevas et al., 2019)..."*

However, the stability of the instrument in the visible+ range for the 3 years period between the manufacturer and the Langley calibrations are impressive. Maybe this also has to be pointed out in the text.

Authors: We have added this information in the final manuscript as follows:

*“...The comparison between the factory calibration performed by EKO Instruments in 2016 and the IZO Langley-Plot calibration (2019) is shown in Figure 7. These results indicate that the stability of the EKO MS-711 in the range 300-1100 nm during a 3 years period, between the manufacturer lamp calibration and the Langley calibrations at IZO, is remarkable...”*

### Circumsolar radiation

Circumsolar radiation contribution to the “true” measured direct irradiance is linked with AOD and also with aerosol types (phase functions). Higher AODs and forward scattering aerosols would introduce higher circumsolar correction factors. As in this work it is mentioned that a mixed (OPAC) based aerosol type is used, have you tested the actual correction and the effect on the AOD retrievals on a day with very high AOD and forward scattered aerosol type (e.g. dust aerosols) ?

Authors: Yes. We have tested/validated the circumsolar radiation correction for dust and for different AOD intervals in the AOD range that we have been able to measure at IZO (up to 0.2). The results are shown in Figures 9 and 10 of the manuscript. Validations for data corrected by CSR are shown in blue

### **Line 41 GAW-PFR showing lower values**

Authors: Done

### **Table 1 : cosine response : is that applicable to the DNI spectral measurements ?**

Authors: No. It is not applicable to DNI measurements. The specifications given in Table 1 correspond to EKO MS-711 spectroradiometer measuring the global solar spectral radiation.

### **Lines 108-110: is this for direct or global irradiance?**

Authors: It is for global irradiance

### **Lines 212: 0.09”**

Authors: Done

### **Congratulations for a very interesting work.**

Authors: Thank you very much for your comment.

# **Characterization of an Aerosol retrievals from the EKO MS-711 spectroradiometer: aerosol retrieval from spectral direct irradiance measurements and corrections of the circumsolar radiation.**

Rosa Delia García-Cabrera<sup>1,2</sup>, Emilio Cuevas-Agulló<sup>2</sup>, África Barreto<sup>3,1,2</sup>, Victoria Eugenia Cachorro<sup>1</sup>, Mario Pó<sup>4</sup>, Ramón Ramos<sup>2</sup>, and Kees Hoogendijk<sup>4</sup>

<sup>1</sup>Atmospheric Optics Group, Valladolid University, Valladolid, Spain

<sup>2</sup>Izaña Atmospheric Research Center (IARC), State Meteorological Agency (AEMET), Spain

<sup>3</sup>Cimel Electronique, Paris, France

<sup>4</sup>EKO INSTRUMENTS Europe B.V., The Hague, the Netherlands

**Correspondence:** Emilio Cuevas Agulló  
(ecuevasa@aemet.es)

**Abstract.** Spectral direct UV-Visible normal solar irradiance (DNI) has been measured with an EKO MS-711 spectroradiometer grating spectroradiometer, which has a spectral range of 300-1100 nm, 0.4 nm step, at the Izaña Atmospheric Observatory (IZO, Spain) has been used to determine aerosol optical depth (AOD) at several wavelengths (340, 380, 440, 500, 675 and 870 nm) between April and September 2019 that have been compared with synchronous AOD measurements from a reference 5 Cimel-AERONET (Aerosol RObotic NETwork) sun photometer. The EKO MS-711 has been calibrated at Izaña Observatory using the Langley-Plot method during the study period. Although this instrument has been designed for spectral solar DNI measurements, and therefore has a field of view (FOV) of 5° that is twice that recommended in solar photometry for AOD determination, the AOD differences compared against the AERONET Cimel reference instrument (FOV  $\sim$ 1.2°), are fairly small. The comparison results between AOD Cimel and EKO MS-711 present a root mean square (RMS) of 0.013 (24.6%) 10 at 340, and 380 nm, and 0.029 (19.5%) for longer wavelengths (440, 500, 675 and 870 nm). However, under relatively high AOD, near forward aerosol scattering might be significant because of the relatively large circumsolar radiation (CSR) due to the large EKO MS-711 FOV, resulting in a small but significant AOD underestimation in the UV range. The AOD differences decrease considerably when CSR corrections, estimated from LibRadtran radiative transfer model simulations, are performed, 15 obtaining RMS of 0.006 (14.9%) at 340 and 380 nm, and 0.005 (11.1%) for longer wavelengths. The percentage of 2- minute synchronous EKO AOD – Cimel AOD differences within the World Meteorological Organization (WMO) traceability limits were  $\geq$  96% at 500 nm, 675 nm and 870 nm with no CSR corrections. After applying the CSR corrections the percentage of AOD differences within the WMO traceability limits increased to  $>$  95% for 380, 440, 500, 675 and 870 nm, while for 340 nm the percentage of AOD differences showed a poorer increase from 67% to a modest 86%.

*Copyright statement.* TEXT

One of the most important elements that governs the Earth's climate, and its processes, is the presence of atmospheric aerosols. The most important effect of the presence of aerosols in the atmosphere is the, which produce a significant radiative forcing resulting from light scattering and absorption, and radiation emission. Furthermore Moreover, they act as cloud condensation nuclei, modifying cloud properties. Therefore, it is clear that aerosols should be taken into account (IPCC, 2013). Aerosols effect on the Earth Radiation Balance has been quantified as a cooling of  $-0.45 \text{ W m}^{-2}$ , and  $-0.9 \text{ W m}^{-2}$  when considering the combined effect of both aerosols and clouds. However, the uncertainty of these values is still very high (WMO, 2016), therefore it is necessary to make more efforts to evaluate the aerosol atmospheric content and optical properties, such as the aerosol optical depth (AOD), Ångström exponent (AE), single scattering albedo, size distribution, etc (SSA), scattering coefficient, and absorption coefficient.

The amount of aerosols present in the atmosphere can be addressed using the aerosol optical depth (AOD) that gives the optical attenuation by aerosols in the atmospheric path. The AOD is derived from surface or satellite observations from sun-light attenuation measurements (WMO, 2016) combined with the Lambert-Beer law. This law has been applied to retrieve the extinction of solar radiation (Ångström, 1930, 1961; Shaw, 1983). The AOD is derived through direct sun radiation measurements at different wavelengths with several instruments such as filter radiometers or spectroradiometers, selecting spectral ranges where the influence of trace gases is minor or even negligible (WMO, 2016; Kazadzis et al., 2018a). The World Meteorological Organization (WMO) recommended the following wavelengths for AOD retrieval: 368, 412, 500, 675, 778 and 862 nm, with a bandwidth of 5 nm (WMO, 1986), and the use of instruments with a full opening angle of  $2.5^\circ$ , and a slope angle of  $1^\circ$  (WMO, 2008).

The AOD retrieval with sunphotometers has been addressed in an extensive list of publications (e.g., Schmid et al. (1999); Kazadzis et al. (2014, 2018a); Barreto et al. (2014); Cuevas et al. (2019)) mainly due to the establishment of aerosol measurement networks, such as AErosol RObotic NETwork (AERONET; Holben et al. (1998)), Precision Filter Radiometer Network (GAW-PFR; Wehrli (2000, 2005)), SKYradiometer NETwork (SKYNET; Takamura and Nakajima (2004)) and SURFace RA-Diation Budget Network (SurfRad; Augustine et al. (2008)). Recently, Cuevas et al. (2019) conducted a study comparing AOD from AERONET-Cimel ( $1.2^\circ$  field of view (FOV)) with that from GAW-PFR ( $2.5^\circ$  FOV) showing a difference of  $\sim 3\%$  at 380 nm and  $\sim 2\%$  at 500 nm compared with AERONET-Cimel for AOD  $> 0.1$ , showing GAW-PFR showing lower values. They demonstrated that this difference was due to the higher amount of dust near-forward scattering measured by GAW-PFR because of its larger FOV. On the other hand, the AOD retrievals from ground-based spectroradiometers are scarce and normally limited to the visible (VIS) range (e.g. Cachorro et al. (2000); Estellés et al. (2006)). The reason for this shortfall may be found in the high costs in investment and maintenance of spectroradiometers, and their substantial requirements for calibration compared to sun-photometers. However, spectroradiometers offer the possibility to provide other atmospheric components (e.g.  $\text{O}_3$ ,  $\text{NO}_2$ ,  $\text{SO}_2$ ,  $\text{CH}_4$ , and  $\text{H}_2\text{O}$ , etc) (e.g. Michalsky et al. (1995); Cachorro et al. (1996); Schmid et al. (2001); Barreto et al. (2014); Raptis et al. (2018)).

The first works that attempting to retrieve AOD from spectroradiometers we done by Cachorro et al. (1987) and Ahern et al. (1991), with results based on a few available data. More recently, several works tackled the AOD multi-spectral retrieval from 55 spectroradiometers with larger datasets. Thus, Cachorro et al. (2000) and Vergaz et al. (2005) reported a quantitative characterization of aerosols in Southern Spain. However, they did not provide a comparison with another AOD retrieval method. Kazadzis et al. (2005) and Gröbner et al. (2001) found AOD differences lower than 0.1 at 355 nm and differences between -0.07 and 0.02 at 315.5 316.75 and 320 nm when comparing AOD retrievals performed with Brewer MKIII and Bentham 60 DTM 300 spectroradiometers and Li-cor spectroradiometer, respectively. Estellés et al. (2006) retrieved AOD with a Li-cor spectroradiometers finding differences with Cimel-318 Sun photometers AOD in the 0.01-0.03 (0.02-0.05) range in the VIS range (UV range). Cachorro et al. (2009) compared AOD retrievals from Li-cor and sunphotometer obtaining AOD differences within 0.02 in the range 440-1200 nm. Kazadzis et al. (2018a) presented the results from the fourth WMO filter radiometer comparison for AOD measurements finding an excellent agreement at 500 and 865 nm between PSR (Precision Solar Spectroradiometer; Raptis et al. (2018)) and PFR (Precision Filter Radiometer; Wehrli (2008)) and overestimation from 0.01 to 65 0.03, respectively. López-Solano et al. (2018) compared AOD retrievals from Brewer spectroradiometers, AERONET-Cimel and UV-PFR in the range 300-320 nm at Izaña Observatory, with uncertainties lower than 0.05.

In this paper we contribute to the knowledge of spectral AOD with a comparison between AOD from AERONET-Cimel sun photometer (onwards, Cimel AOD) and AOD computed from the direct normal irradiance (DNI) measurements performed with an EKO MS-711 spectroradiometer (onwards, EKO AOD). We have also addressed the small, but significant, EKO 70 AOD underestimation under relatively high AOD due to dust near-forward scattering, but in this case have compared two instruments whose FOV values show a big difference since the EKO FOV is 5°. We have divided this work into 5 sections: Sect. 2 describes the main characteristics of the Izaña station and the technical description of the instruments used in this work. In Sect. 3 the methodology used to determine AOD and the corrections due to the differences in dust forward scattering, using the LibRadtran radiative transfer model (RTM) and spectral Langley-Plot calibration are described. In Sect. 4 the main results 75 of the comparison are shown. Finally, a summary and the main conclusions are given in Sect. 5.

## 2 Site description, Instrument and ancillary information

### 2.1 Site description

The data used in this work were acquired between April and September 2019 at the Izaña Observatory (IZO). This observatory is located on the island of Tenerife (Spain; 28.3°N, 16.5°W; 2.4 km a.s.l.) and it is approximately 350 km away from the 80 African continent. This observatory is managed by Izaña Atmospheric Research Center (IARC) from the State Meteorological Agency of Spain (AEMET) (more information: <http://izana.aemet.es>; last access: 7 November 2019).

In 1984, IZO enrolled in the WMO Background Atmospheric Pollution Monitoring Network (BAPMoN) and the WMO Global Atmosphere Watch (GAW) program in 1989. IZO collaborates with different international networks such as the Network for the Detection of Atmospheric Composite Change (NDACC) since 1999, and the GAW-PFR since 2001. In 2003, the 85 Regional Brewer Calibration Centre for Europe (WMO/GAW RBCC-E) was established. Furthermore, IZO has been part



**Figure 1.** The EKO MS-711 spectroradiometer installed at IZO.

of AERONET since 2004, as one of the two AERONET Langley-Plot calibration sites (Toledano et al., 2018). Since 2009, IZO runs a Baseline Surface Radiation Network (BSRN) station. In 2014, IZO was appointed by WMO as a Commission for Instruments and Methods of Observation (CIMO) Testbed for aerosols and water vapor remote sensing instruments (WMO, 2014). More details of IZO programs can be found in Cuevas et al. (2017).

## 90 **2.2 Instrument: EKO MS-711 spectroradiometer**

An EKO MS-711 grating spectroradiometer used in direct sun measurement mode has been tested (Figure 1) within the CIMO Testbed program from April to September 2019 (14706 datapoints).

The EKO MS-711 was designed to measure global solar spectral radiation within the 300 and 1100 nm wavelength range with an average step of  $\sim 0.4$  nm, exhibiting a full-width-at-half-maximum (FWHM)  $< 7$  nm. It is equipped with its own built-in entrance optics, and the housing is temperature-stabilized at  $25^\circ \pm 5^\circ$  (Egli et al., 2016). EKO Instruments designed a collimator tube that also allows measuring DNI (see Figure 1).

This spectroradiometer has been mounted on an EKO sun-tracker STR-21G-S2 (accuracy of  $< 0.01^\circ$ ). This setup performs DNI measurements each 1-minute one spectrum per minute, with an exposure time that changes automatically according to the intensity of the irradiance that varies from 10 ms to 5 s. The main specifications of the EKO MS-711 spectroradiometer are 100 shown in Table 1.

**Table 1.** Main specifications of the EKO MS-711 spectroradiometer.

Wavelength range	300 to 1100 nm
Wavelength interval	0.3 - 0.5 nm
Optical resolution FWHM	< 7nm
Wavelength accuracy	± 0.2 nm
Cosine response (zenith: 0-80°)	< 5 %
Temp. dependency (-10 °C to 50 °C)	< 2 %
Temp. control	25 °C ± 2 °C
Operating temperature	-10 to 50 °C
Exposure time	10 ms <sup>-5</sup> sec Automatic adjustment
Dome material	Synthetic Quartz Glass
Communication	RS-422 (Between sensor and power supply)
Power requirement	12VDC, 50VA (from the power supply)
Full opening angle (FOV)	5°

### 2.3 Ancillary Information: Cimel sun-photometer/AERONET

In this work, we have used AOD data provided by the AERONET permanent Cimel CE318 reference instrument to compare the AOD derived with the EKO MS-711 spectroradiometer. The different Cimel ~~referencee~~references have been shown to have a good ~~AOD~~ traceability with the ~~world AOD GAW-PFR worldwide~~ reference (Cuevas et al., 2019). The world AOD reference

105 is maintained by the World Optical Depth Research and Calibration Center (WORCC) (Kazadzis et al., 2018b).

The Cimel CE318 photometer is an automatic sun-sky scanning filter radiometer that measures AOD at 340, 380, 440, 500, 675, 870 and 1020 nm (nominal wavelength; extended wavelength versions additionally have 1640 nm) with a full opening angle of 1.2°. The uncertainty in AOD measurements from Cimel field instruments, was estimated to be ± 0.01 in the VIS range and near-IR, increasing to ± 0.02 in the UV range (340 and 380 nm) (Eck et al., 1999). This estimate gives an absolute

110 bias < 0.01 for AOD lower than 1.5 (Sinyuk et al., 2012). In this ~~work~~study, we have used ~~eloud~~-screened and quality-assured AERONET Version 3.0 Level 1.5 AOD data.

## 3 Methodology

### 3.1 Spectral Langley Calibration

The EKO MS-711 spectroradiometer was factory calibrated by EKO Instruments making use of a calibrated transfer standard

115 1000 W quartz tungsten-halogen coiled-coil filament lamp that is traceable to the National Institute of Standards and Technology (NIST) standard (Yoon et al., 2000). The instrument resultant uncertainty is ± 17% for the UV range, and < 5% for the VIS range. In November 2016, the EKO MS-711 participated in an intercomparison campaign of spectroradiometers at the National

Oceanic and Atmospheric Administration (NOAA) Mauna Loa observatory, Hawaii Island, USA (19.54° N, 155.58° W; 3397 m a.s.l.) (Pó et al., 2018), where it was calibrated with the Langley method (Ångström, 1970; Shaw et al., 1973; Shaw, 1983).

120 In 2018 the instrument was deployed at the World Radiation Center- Physical Meteorological Observatory (WRC-PMOD) for its characterization using a tunable laser (Sengupta et al., 2019). Recently, between April and September 2019, the EKO MS-711 has been calibrated at Izaña Observatory using the Langley method in the 300-1100 nm spectral range. In this study we have used the calibration coefficients with the Langley-Plot method.

The Langley method used in the IZO Langley calibration is based on the Beer-Lambert-Bouguer law:

125 
$$DNI(\lambda) = DNI_o(\lambda)e^{-\tau(\lambda)m} \quad (1)$$

where  $DNI(\lambda)$  is the direct normal irradiance at wavelength  $(\lambda)$  measured by the instrument,  $DNI_o(\lambda)$  is the top-of-atmosphere irradiance corrected for the Sun-Earth distance at wavelength  $(\lambda)$ ,  $m$  is air mass, and  $\tau(\lambda)$  is the optical depth that can be written in the UV-VIS range as:

$$\tau(\lambda) = \tau_R(\lambda) + \tau_a(\lambda) + \tau_{NO_2}(\lambda) + \tau_{H_2O}(\lambda) + \tau_{O_2}(\lambda) + \tau_{O_3}(\lambda) \quad (2)$$

130 where  $\tau_R(\lambda)$  is the Rayleigh optical depth (Hansen and Travis, 1974) due to the molecular scattering that depends on the station pressure as well as on the optical air mass ( $m_R$ ) (Bodhaine et al., 1999),  $\tau_a(\lambda)$  is the AOD, and the rest of the terms are the absorption by atmospheric gases in the affected wavelengths (Gueymard, 2001) and are defined as follows:

$$\tau_R = \frac{P}{P_o} 0.008569 \lambda^{-4} (1 + 0.0113 \lambda^{-2} + 0.00023 \lambda^{-4}) \quad (3)$$

where  $P$  is the pressure at the measurement site within the earth's atmosphere,  $P_o$  is the standard pressure at sea level and  $\lambda$  is

135 the wavelength in  $\mu\text{m}$ . In-situ actual pressure at IZO was used.

$$\tau_{NO_2}(\lambda) = u_{NO_2} A_{NO_2} \quad (4)$$

where  $u_{NO_2}$  is the reduced path-length (in atm-cm) taken from the OMI total column  $NO_2$  monthly average climatology and  $A_{NO_2}$  its spectral absorption coefficient (Rothman et al., 2013).

$$\tau_{H_2O}(\lambda) = (u_{H_2O} A_{H_2O})^{\frac{b}{b_{H_2O}}} \quad (5)$$

140 where  $u_{H_2O}$  is the column water vapour content (precipitable water) taken from a Global Navigation Satellite System (GNSS) receiver considering satellite precise orbits at IZO (Romero Campos et al., 2009),  $A_{H_2O}$  the spectral absorption coefficient Rothman et al. (2013), and the  $\frac{b}{b_{H_2O}}$  exponent depends on the central wavelength position, instrument filter function, as well as the atmosphere pressure and temperature (Halthore et al., 1997). We have determined  $\tau_{H_2O}(\lambda)$  from the transmittance for different water vapour and solar zenith angle (SZA) values from the MODTRAN model (Raptis et al., 2018).

$$145 \quad \tau_{O_2}(\lambda) = (u_{O_2} A_{O_2})^{\frac{b}{b_{O_2}}} \quad (6)$$

where  $u_{O_2}$  is the altitude-dependent gaseous scaled path-length taken from the Fourier transform infrared spectrometer (FTIR) measurements at IZO (Schneider et al., 2005),  $A_{O_2}$  is the spectral absorption coefficient (Rothman et al., 2013), and the  $b_{O_2}$  exponent was obtained from the transmittance values simulated with the MODTRAN model (Berk et al., 2000) for IZO, obtaining a value of 0.454. This value is similar to that obtained by Pierluissi and Tsai (1986, 1987).

150 
$$\tau_{O_3}(\lambda) = \underline{(u_{O_3} A_{O_3})^b} \quad (7)$$

where  $u_{O_3}$  is the total column ozone obtained with a reference Brewer spectrophotometer at IZO (Redondas et al., 2018), and  $A_{O_3}$  the ozone absorption cross section (Brion et al., 1993, 1998).

The Langley-Plot determines  $DNI_o(\lambda)$  (that allows to derive calibration constant) from a linear extrapolation of  $DNI(\lambda)$  measurements to zero air mass, corrected to mean Sun–Earth distance, and plotted on a logarithmic scale versus air mass:

155 
$$\ln DNI(\lambda) = \ln DNI_o(\lambda) - [\tau_R(\lambda) \underline{m_R} + \tau_a(\lambda) \underline{m_a} + \tau_{NO_2}(\lambda) \underline{m_{NO_2}} + \tau_{H_2O}(\lambda) \underline{m_{H_2O}} + \tau_{O_2}(\lambda) \underline{m_{O_2}} + \tau_{O_3}(\lambda) \underline{m_{O_3}}] \quad (8)$$

where the different air masses have the following expressions:

$$\underline{\underline{m_R \sim m_{O_2} = \frac{1}{\cos(\theta) + 0.50575(96.07995 - \theta)^{-1.6364}}}}; \text{(Kasten and Young, 1989; Gueymard, 2001)} \quad (9)$$

$$\underline{\underline{m_a \sim m_{H_2O} = \frac{1}{\cos(\theta) + 0.0548(92.65 - \theta)^{-1.452}}}}; \text{(Kasten, 1966)} \quad (10)$$

160

$$\underline{\underline{m_{NO_2} = \frac{1}{\sin(\theta) + 602.30(90 - \theta)^{0.5}(27.96 + \theta)^{-3.4536}}}}; \text{(Gueymard, 1995)} \quad (11)$$

$$\underline{\underline{m_{O_3} = \frac{R + h}{\sqrt{(R + h)^2 - (R + r)^2 \sin^2(\theta)}}}}; \text{(Komhyr et al., 1989)} \quad (12)$$

where  $R$  (6370 km) is the mean radius of the Earth,  $r$  is the station height above mean sea level in km, and  $h$  is the mean height of the ozone layer in km (22 km).

### 3.2 AOD retrieval method

The AOD retrievals have been calculated from Eq. 8, as follows:

$$AOD = \frac{1}{m_a} [\ln DNI_o(\lambda) - \ln DNI(\lambda) - \tau_R m_R - \underline{(\tau_{NO_2}(\lambda) \underline{m_{NO_2}} + \tau_{H_2O}(\lambda) \underline{m_{H_2O}} + \tau_{O_2}(\lambda) \underline{m_{O_2}} + \tau_{O_3}(\lambda) \underline{m_{O_3}})}] \quad (13)$$

If we group Grouping the gases contributions such as  $\tau_{gas}$ , the AOD expression is reduced to:

170 
$$AOD = \frac{1}{m_a} [\ln DNI_o(\lambda) - \ln DNI(\lambda) - \tau_R m_R - \tau_{gas} m] \quad (14)$$

**Table 2.** Wavelengths characteristics of Cimel and spectral corrections used in the calculation of AOD.

Nominal central wavelength (nm)	Filter Bandpass (nm)	Spectral Corrections
340	2	Rayleigh, NO <sub>2</sub> , O <sub>3</sub>
380	4	Rayleigh, NO <sub>2</sub>
440	10	Rayleigh, NO <sub>2</sub>
500	10	Rayleigh, NO <sub>2</sub> , O <sub>3</sub>
675	10	Rayleigh, O <sub>3</sub>
870	10	Rayleigh

In this work, we have calculated the EKO AOD at the same nominal wavelengths as those of the Cimel (340, 380, 440, 500, 675 and 870 nm), by integrating the measured irradiance on the considered bandpass (see Table 2), following the methodology used by AERONET (Holben et al. (2001); Giles et al. (2019), and references herein). For this each wavelength, we have taken into account the spectral corrections shown in Table 2. The All wavelengths have been corrected by the Rayleigh scattering (see Sect. 3.1). Furthermore the 340, 380, 440 and 500 nm wavelengths are corrected from nitrogen dioxide (NO<sub>2</sub>) absorption, and being the optical depth is calculated using the OMI total column NO<sub>2</sub> OMI monthly average climatology climatological monthly averages, and the NO<sub>2</sub> absorption coefficient from Burrows et al. (1999). The 340, 500 and 675 nm channels are corrected of ozone, using the ozone values from the Izaña WMO-GAW reference Brewer spectroradiometer.

### 3.3 Corrections in AOD under relatively high CSR

The full opening angle and the FOV are normally used indistinctly in the literature, which should not be confused with the viewing angle. Therefore, we use the term FOV for referring to the full opening angle. As we remarked in the introduction, the WMO recommended for AOD retrieval the use of instruments with FOV lower than 2.5° and slope angle of 1° (WMO, 2008). As the EKO MS-711 was designed for DNI measurements, it has a larger FOV of 5°, twice the WMO recommended value for AOD retrievals. To account for the different geometries, we have applied a correction to the EKO irradiance measurements. In this section we explain the methodology applied to the measurements and comparisons with Cimel AOD.

The DNI measurement implies that a certain amount of diffuse radiation coming from the line-of-sight of the instrument towards the Sun, and an annular region around it, the so-called circumsolar region, is measured together with the DNI coming from the Sun disk ( $DNI_{SUN}$ ). The source of this diffuse radiation, CSR (circumsolar radiation), lies on the scattering processes due to the presence of aerosols and clouds (Blanc et al., 2014) in the atmosphere. This CSR has a high dependence on particle size the aerosol scattering phase function (Räisänen and Lindfors, 2019) and leads to overestimate on the particle size (Räisänen and Lindfors, 2019), thus large particles (such as desert dust) produce a higher scattering on the incident beam than the smaller particles (e.g., rural background aerosols), leading this contribution to overestimate the DNI. Thus, the experimental DNI measured by a collimated instrument maybe expressed as the sum of both contributions:

$$DNI = DNI_{SUN} + CSR \quad (15)$$

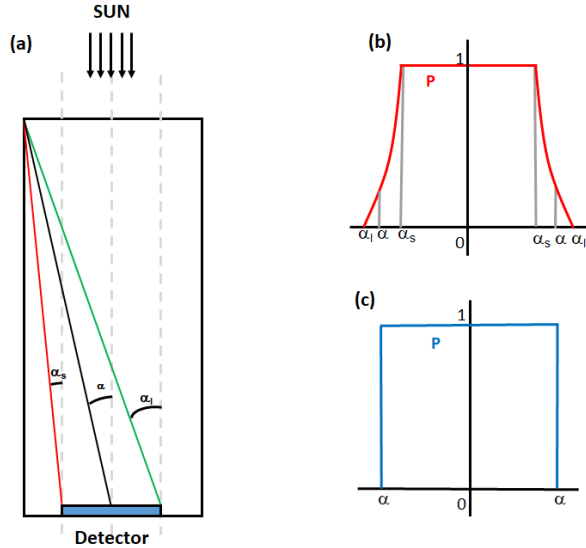


**Figure 2.** (a) Characteristic angles of the instrument: slope angle  $\alpha_s$ , aperture half-angle  $\alpha$  and limit angle  $\alpha_l$ . On the right, penumbra functions  $P(\alpha)$  when (b) the three angles are known and (c) if only the half-angle angle is known. (Figure adapted from Blanc et al. (2014)).

195 where  $DNI_{SUN}$  is the direct normal irradiance coming from the Sun disk and CSR is the diffuse radiation coming from the sky that is seen by the instrument FOV. This FOV is defined by the instrument geometry and determines the amount of CSR reaching the instrument detector. The value of the DNI measured by the instrument also depends on the atmospheric conditions, and the specific instrument characteristics. The most important element that defines the amount of CSR captured by the instrument is the penumbra function  $P$  (Pastiels, 1959) that defines the fraction of Sun radiation captured or not by the collimator, depending  
200 on its angle of vision. This penumbra function can be derived from geometrical features of the instrument (Major, 1980; Blanc et al., 2014): the aperture half-angle  $\alpha$ , the slope angle  $\alpha_s$  and the limit angle  $\alpha_l$  (Fig. 2a). Usually the three angles are known, being the most important the aperture half-angle  $\alpha$ . Thus, the radiation coming from the sky with an angle higher than the  $\alpha_l$  is outside the collimator and then not measured by the instrument.

205 If all angles are known the function  $P$  takes the shape of Figure 2b, but if  $\alpha_s$  and  $\alpha_l$  are unknown, the penumbra function  $P$  can be approximated as the shape on Figure 2c. In this work, we used the penumbra function  $P$  described in Figure 2c, because  $\alpha_s$  and  $\alpha_l$  are unknown, and considering that  $\alpha = \text{FOV}/2 = 2.5^\circ$ .

### 3.4 CSR simulation

210 Since it is not possible to obtain accurate CSR measurements, it has been simulated with the LibRadtran radiative transfer model (Mayer and Kylling (2005); Emde et al. (2016), more information <http://www.libradtran.org>; last access: 7 November 2019), which provides the possibility to simulate the diffuse radiance on sky elements defined by its azimuthal and polar angles.

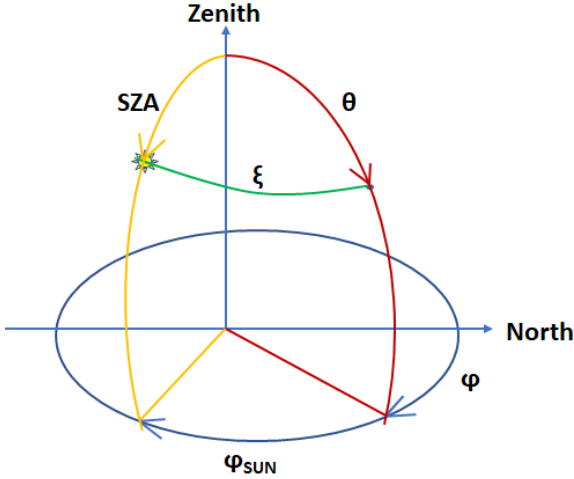


**Figure 3.** Geometry of the problem. The Sun is located in the coordinates (SZA,  $\varphi_{SUN}$ ) and the sky point is in  $\theta, \phi$ . The instrument is located in the origin of the axes.

We shortly describe the method followed to simulate the amount of CSR measured by the EKO MS-711. The first step is to describe the geometry of the problem, shown in Figure 3.

For a sky point defined by the polar angle  $\theta$  and azimuthal angle  $\varphi$ , the sky radiance on that point is  $L(\theta, \varphi)$  in  $\text{W m}^{-2}\text{sr}^{-1}$ . The angular distance between the considered point and the Sun position (the green arc in Figure 3), is the so-called scattering angle,  $\xi$ . To obtain the angle  $\xi$  of each point on the sky in terms of the polar and azimuthal angles the next equation should be used:

$$\cos(\xi) = \cos(SZA)\cos(\theta) + \sin(SZA)\sin(\theta)\cos(\varphi - \varphi_{SUN}) \quad (16)$$

Taking into account this relation, the radiation field  $L$  can be expressed in terms of  $\xi$  and  $\varphi$ , thus the irradiance in the solid angle subtended by an angular distance from the Sun's centre  $\xi$ , for an instrument with an aperture half-angle  $\alpha$ , is (Blanc et al., 2014):

$$I = \int_0^{2\pi} \int_{\alpha_o}^{\alpha} P(\xi, \varphi) L(\xi, \varphi) \cos(\varphi) \sin(\xi) \cdot d\varphi d\xi \quad (17)$$

where  $P(\xi, \varphi)$  is the penumbra function defined in Sect. 3.3. If the Sun is in the angular field considered, the obtained irradiance is the DNI of Eq. 15, if not, the result will be only the diffuse radiation. Thus, the key is to simulate the radiances  $L(\xi, \varphi)$  of the points in the FOV that the instrument is “seeing”. In this work, and taking into account that the instrument is continuously pointing to the Sun, the integration is performed for  $\xi$  values from  $\alpha_o = 0.6^\circ$  to  $\alpha = 2.5^\circ$  with the aim to simulate the diffuse radiation coming from a circumsolar ring, in order to compare AOD from both instruments using the same CSR.

The input parameters used in the simulations are shown in Table 3. The aerosol contribution has been included in the simulations by using the Optical Properties of Aerosols and Clouds (OPAC package) (Hess et al., 1998). This library provides

**Table 3.** The inputs to LibRadtran model used in this work.

Parameters	Input	Reference
Aerosol parameters	OPAC	Hess et al. (1998)
AOD	AOD estimated from EKO MS-711	-
Altitude	2.4 km	-
Absorption Parameterization	REPTRAN (fine resolution)	Gasteiger et al. (2014)
Atmosphere profile	Midlatitude summer	Anderson et al. (1986)
Solar flux	Kurucz (0.1 nm resolution)	Kurucz (1994)
Slit function	Function Gaussian function with FWHM of 6-7 nm	-
Radiative transfer equation solver	DISORT, with spherical correction for SZA > 60°	Stamnes et al. (1988)
Surface Albedo	0.11	García et al. (2014)
Ozone Column	Ozone column performed with Brewer spectroradiometer at IZO	-
Number of streams	8	-

the aerosol (and clouds) optical properties in the range 250 nm to 4000 nm. In our case, we focused the interest in the aerosol mixtures, due to the fact the aerosols in the atmosphere are found as a mixture of different particles. In the LibRadtran package are included the aerosol mixtures described in Hess et al. (1998). The aerosol optical properties stored in the datasets used are: the extinction coefficient, scattering coefficient, absorption coefficient, volume phase function, single scattering albedo and asymmetry parameter. Due to the location of the IZO station we have selected the desert mixtures for the cases of low and high aerosol load **respectively**.

At this point we should note that the use of 1D simulations with the DISORT (Stamnes et al., 1988) solver implies that the Sun is supposed to be a Dirac function, while, the Sun has an angular radius of  $960.12'' \pm 0.09''$  (Emilio et al., 2012). However, Stamnes et al. (1988) demonstrated that the error in  $DNI_{SUN}$  simulations, when the Sun is assumed to be a point source, is negligible with respect to the finite Sun assumption (Stamnes et al., 2000; Reinhardt, 2013) showed that the simulations of radiances in the vicinity of the Sun performed using the DISORT and OPAC aerosols for cloud-free cases give the same result than simulations made with the Monte-Carlo RTE solver MYSTIC included in LibRadtran (Mayer, 2009) taking into account the angular extent of solar disk. The differences remain under 1% and even very close to 0%. Since we want to simulate cloud-free cases, we can use the 1D, DISORT without introducing significant errors in the simulations against the more precise Monte-Carlo simulations.

Once we have selected the input parameters, we must also select the correct angular grid in azimuthal and polar coordinates to cover, at least, the angular region previously defined ( $0.6^\circ \leq \alpha \leq 2.5^\circ$ ). By using Eq. 16 we can calculate the ranges of polar angles  $\theta$  and azimuthal angles  $\varphi$  needed. The result of a monochromatic simulation, i.e.  $L(\xi, \varphi)$  at 495 nm for the day

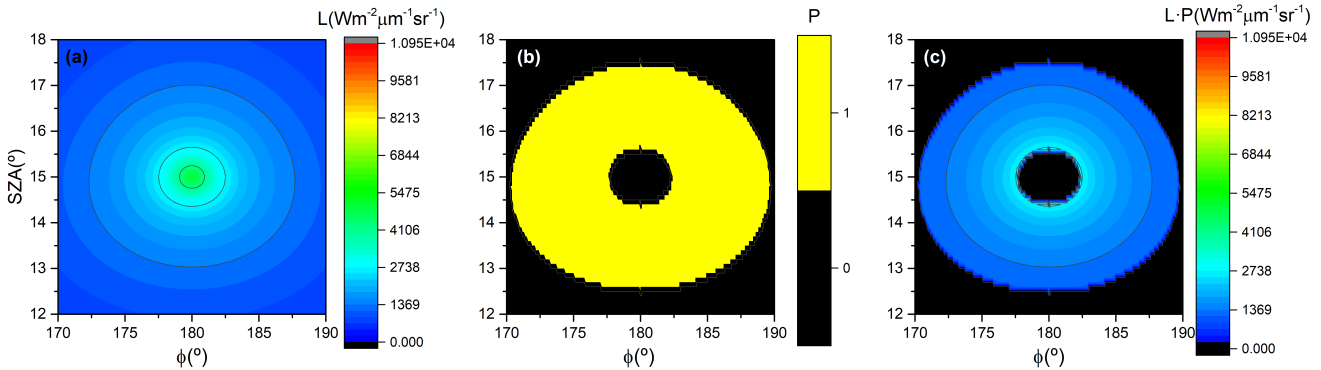


**Figure 4.** Example of the (a) diffuse radiance  $L$  ( $\text{Wm}^{-2}\mu\text{m}^{-1}\text{sr}^{-1}$ ) at 500 nm shown in colours at different SZA and  $\varphi$  (b) penumbra function  $P$  determined from Eq 16 and (c) the product of the diffuse radiance  $L$  and penumbra function  $P$ .

26/07/2019 at SZA of  $\sim 14^\circ$  is shown in Figure 4a. In Figure 4b the penumbra function, i.e.  $P(\xi, \varphi)$  is shown, and in Figure 4c, the result of multiply  $P(\xi, \varphi)$   $L(\xi, \varphi)$ . Note that the angular grid has been selected in steps of  $0.1^\circ$ .

The expected CSR will be obtained by integrating the radiation field  $P(\xi, \varphi)$   $L(\xi, \varphi)$  as indicated in Eq 17. The integration 250 is done by using the angres tool (Mayer and Kylling, 2005) provided in the LibRadtran package which uses a Monte Carlo integration in 2D to obtain the diffuse radiation in the considered radiation field.

### 3.5 AOD retrievals with CSR corrections

Once the CSR has been determined, we apply the correction to the measured DNI taking into account the CSR simulations explained before. Thus, from Eq. 15 the corrected DNI is:

$$255 \quad DNI_{CORR} = DNI_{\text{SUN}} - CSR \quad (18)$$

This correction will lead to a  $DNI_{CORR} < DNI$ , with which we can retrieve an AOD with a similar expression to Eq. 14:

$$AOD_{CORR} = \frac{1}{m_a} [\ln DNI_{oCORR}(\lambda) - \ln DNI_{CORR}(\lambda) - \tau_R m_R - \tau_{gas} m] \quad (19)$$

We must note on Eq. 19 that  $DNI_o$ , calculated with the Langley-Plot calibration method (see Sec. 3.1), should be also calculated applying a FOV correction using Eq. 8, by substituting  $DNI_o$  with the corrected  $DNI_{oCORR}$ . The EKO  $AOD_{CORR}$  260 obtained from Eq. 19 with a  $DNI_{oCORR}$  calculated from Eq. 18 is supposed to be “free” of any CSR contribution, then it is straight forward to assume that the  $AOD_{CORR}$  is closer to the real AOD present in the atmosphere. In order to know the impact of the aerosol load and the FOV size in the values of the CSR simulations we have calculated the ratio of the simulated CSR with respect to the DNI given by Eq. 15, this is the so-called circumsolar ratio (CR) under cloud-free conditions. We have done simulations of  $DNI_{SUN}$  and CSR to obtain the previously cited CR, varying the aerosol load in the range [0-0.50] and

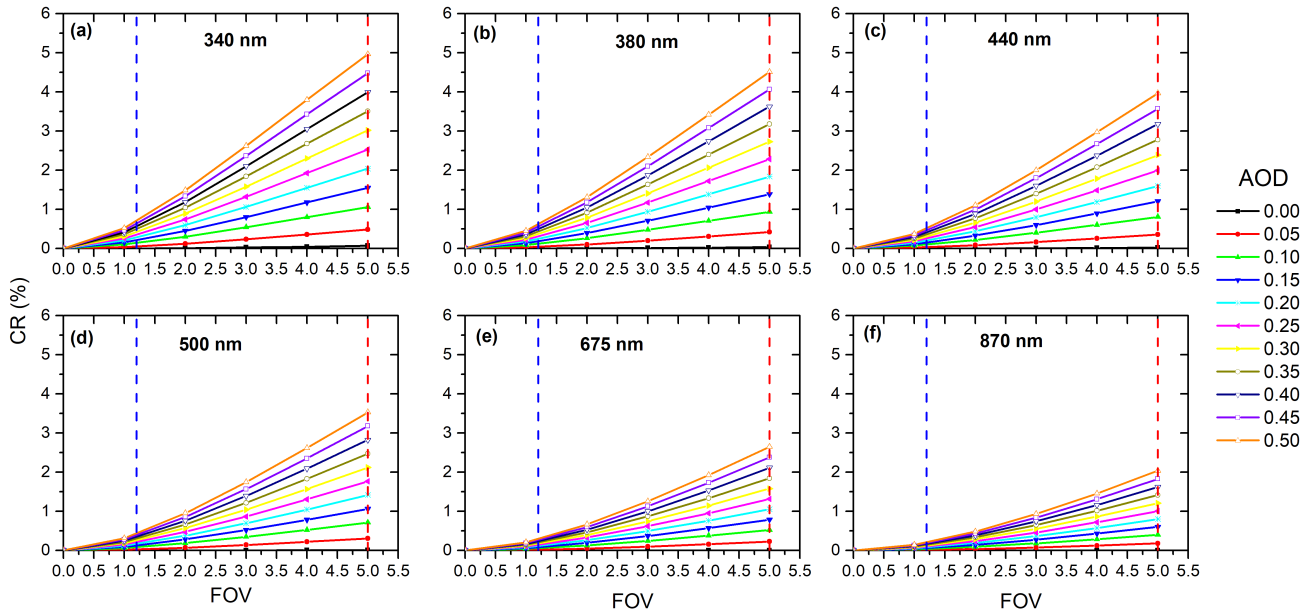


**Figure 5.** Simulations of CR at (a) 340, (b) 380, (c) 440, (d) 500, (e) 675 and (f) 870 nm for AOD between 0.0 and 0.50 and FOV between 0° and 5° at SZA 30°. The dashed blue and red lines represent the Cimel FOV (1.2°) and EKO MS-711 FOV (5°), respectively.

265 the FOV in the range [0°–5°]. The rest of the input parameters remain fixed. The results of CR in percentage (Neumann and Witzke, 1999) for a solar zenith angle of 30° is shown for the six Cimel channels in Figure 5.

$$\text{CR}(\%) = \frac{CSR}{DNI_{SUN} + CSR} * 100 \quad (20)$$

As can be seen in Figure 5, CR increases for higher FOV and larger AOD, as expected, and for the lower wavelengths. The dashed lines in Figure 5 indicate the FOV of the instruments used in this work Cimel (blue line) and EKO (red line). The CR 270 for the Cimel in all cases is lower than 1% and even 0.5% for the channels over 440 nm. For EKO the CR ranges between 2% in the 870 nm channel and 5% for the 340 nm channel. Thus, the expected CSR maximum values in Figure 5 should be found at these conditions: FOV of 5°, AOD of 0.50 and wavelength of 340 nm, in which a CR of 5% is found. We have simulated the AOD retrievals as a function of CSR. By combining Eq. 18 to 2420, we can vary CR (in fact the value of CSR) and calculate the AOD retrieved with the corresponding  $DNI_{OCORR}$ .

275 These results indicate that the CSR impacts significantly on the EKO AOD retrievals under relatively high AOD leading to AOD underestimation, with this effect being less important for the Cimel AOD retrievals because of its narrower FOV.

These results have been simulated considering the typical conditions of IZO where mineral dust is practically the only aerosol present (Berjón et al., 2019; García et al., 2017). Simulations of the effect on CR of the eight OPAC mixture aerosols

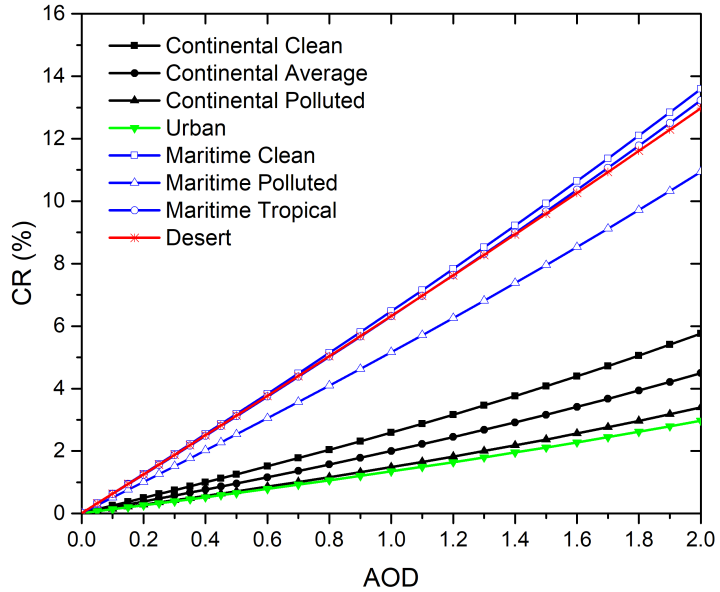


**Figure 6.** Simulations of CR (%) for SZA 30° at sea level for AOD values between 0 and 2, at 500 nm, for different types of aerosols for FOV of 5°.

available in LibRadtran model, continental (clean, average and polluted), urban, maritime (clean, polluted and tropical) and desert aerosols (Hess et al., 1998), and for a FOV=5°, are shown in Figure 6. For SZA=30°, with an  $AOD_{500\text{nm}}$  range between 0 and 2 at sea level, two defined groups are distinguished: the continental and urban aerosol mixtures, and the maritime and desert dust mixtures. It should be noted that for stations located in urban or continental (clean and contaminated) environments, which are the majority, the correction that would have to be made to the AOD for a very high aerosol load (e.g.,  $AOD = 1$ ) would be much lower, between 1/3 to 1/6, than the correction that would have been performed in the case of dust aerosol. (Figure 6 and Appendix B).

## 4 Results

### 4.1 Langley calibration at Izaña Observatory

Based on the experience of Kiedron and Michalsky (2016) and Toledano et al. (2018), we have considered that the Langley calibration is suitable if the standard deviation ( $\sigma$ ) of the fit (Eq. 8) is lower than 0.006, the correlation coefficient ( $R$ ) > -0.99, the number of valid points > 33% of the initial sample, and  $AOD$  (500 nm) < 0.025. In order to test the Langley method

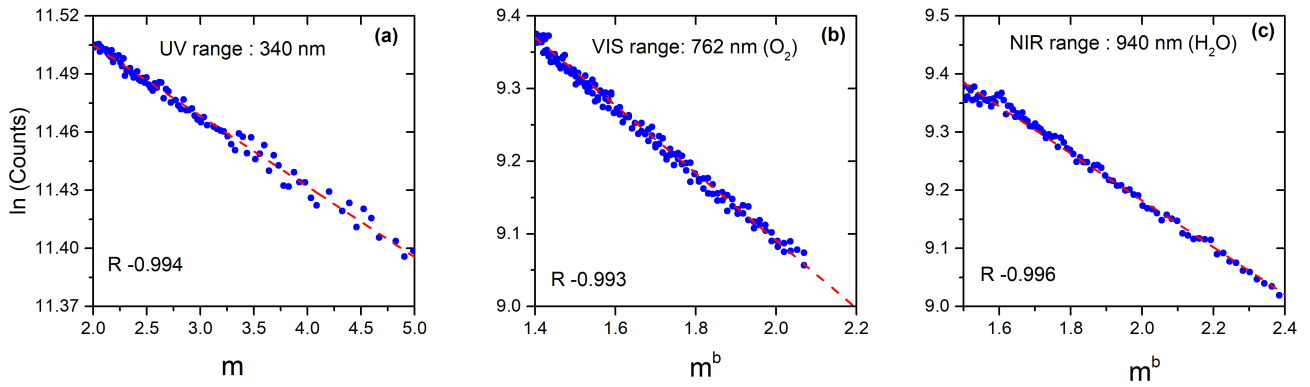


**Figure 7.** Examples of Langley-Plots using the UV-VIS-near IR direct-Sun measurements on 19 March 2019 at Izaña Observatory at (a) 340 nm, (b) 762 nm ( $O_2$ ) and (c) 940 nm ( $H_2O$ ) nm. R: correlation coefficient.

described in Sect. 3.1, an example of Langley-Plots using the UV-VIS-near IR direct-Sun measurements on 19 March 2019 at Izaña Observatory are shown in Figure 7.

The comparison between the factory calibration performed by EKO Instruments in 2016 and the IZO Langley-Plot calibration (2019) is shown in Figure 8. ~~This results indicate a high stability of~~ ~~These results indicate that the stability of the~~ ~~EKO~~ 295 ~~MS-711~~ ~~in the range 300-nm—1100 nm, in the last 300–1100 nm during a 3 years period, between the manufacturer lamp calibration and the Langley calibrations at IZO, is remarkable~~. The factory calibration and the IZO Langley-Plot calibration three years later present differences  $\sim 4.8\%$  between 350 and 1100 nm and even  $\leq 2.3\%$  and  $3.1\%$  in the VIS and near-IR range, respectively. The larger differences below 350 nm are attributed to the low halogen lamp signal in this region experienced during the factory calibration, and low instrument sensitivity in this region.

300 Applying the previous method,  $DNI_o(\lambda)$  values and their standard deviations from the EKO MS-711 measurements (from April to September 2019 at Izaña Observatory) at the nominal wavelengths measured by the Cimel (340, 380, 440, 500, 675 and 870 nm), as a function of time are shown in Figure 9. These  $DNI_o(\lambda)$  values have been used in the AOD retrievals.

#### 4.1.1 AOD retrievals

In this section, we present the results obtained when comparing Cimel AOD and EKO AOD with no CSR corrections (CSR uncorrected AOD) and applying a CSR correction (CSR corrected AOD). The comparisons were done considering measurements of both instruments that match within 2 minutes for all wavelengths. This approach produced a Cimel and EKO AOD dataset with a total of 14706 quasi-coincident measurements. The results show (Table 4) that there is a good agreement ~~(correlation coefficient > 0.98)~~ between EKO AOD and Cimel AOD for all channels, even for no CSR correction, except for the lowest 340 nm UV channel.

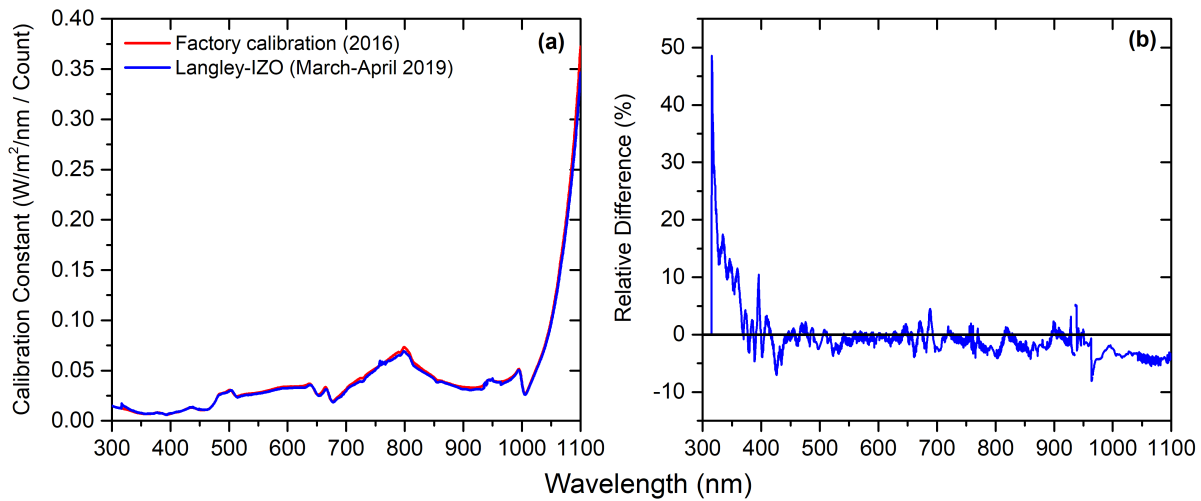


**Figure 8.** (a) Calibration constants ( $\text{W m}^{-2}/\text{nm}/\text{Count}$ ) of the EKO MS-711 spectroradiometer, and (b) relative differences between factory calibration constants and those obtained from Langley-Plots at IZO.

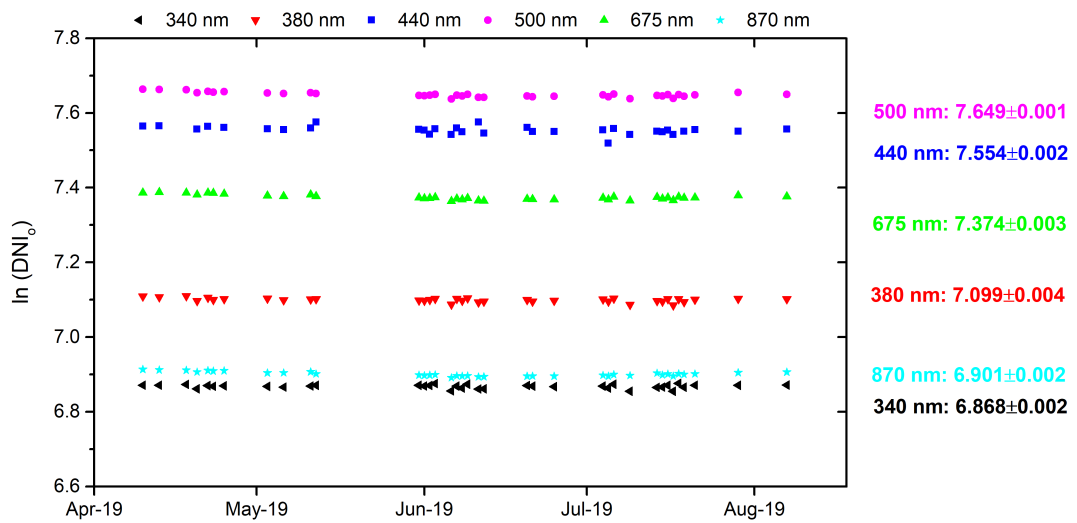


**Figure 9.** EKO MS-711  $DNI_o(\lambda)$  values, and corresponding standard deviations, between April and September 2019 at IZO, for all nominal wavelengths measured by the Cimel (340, 380, 440, 500, 675 and 870 nm).

**Table 4.** Statistics of the comparison between EKO AOD, with no CSR corrections ([CSR Unc.](#)) and implementing CSR corrections ([CSR Corr.](#)), and Cimel AOD at 340, 380, 440, 500, 675 and 870 nm at IZO between April and September 2019. R: correlation coefficient, slope of the least-squares fit between EKO AOD and Cimel AOD, RMS: root mean square of the bias and MB: mean bias. The results of the relative bias are in brackets (in %).

Wavelength (nm)	R		Slope		RMS		MB	
	CSR Unc.	<a href="#">CSR UncCorr.</a>						
<b>340 nm</b>	0.960	0.973	1.063	0.994	0.017	0.007	0.015	<0.001
					(28.9%)	(16.9%)	(24.5%)	(-1.4%)
<b>380 nm</b>	0.981	0.986	1.071	1.001	0.009	0.005	0.007	<0.001
					(20.2%)	(12.9%)	(14.8%)	(1.2%)
<b>UV-Range</b> <b>(Mean)</b>	0.971	0.979	1.067	0.997	0.013	0.006	0.011	<0.001
					(24.6%)	(14.9%)	(19.7%)	(1.3%)
<b>440 nm</b>	0.984	0.987	1.041	0.997	0.101	0.005	0.009	0.001
					(22.4%)	(13.5%)	(18.7%)	(0.6%)
<b>500 nm</b>	0.988	0.991	1.075	1.018	0.007	0.005	0.004	0.002
					(18.2%)	(12.9%)	(12.1%)	(0.4%)
<b>675 nm</b>	0.989	0.991	1.057	1.013	0.006	0.006	0.003	<0.001
					(19.7%)	(10.7%)	(11.2%)	(0.5%)
<b>870 nm</b>	0.998	0.999	1.039	1.009	0.004	0.003	<0.001	<0.001
					(18.8%)	(7.3%)	(0.3%)	(0.2%)
<b>VIS-Range</b> <b>(Mean)</b>	0.989	0.992	1.053	1.009	0.029	0.005	0.004	<0.001
					(19.5%)	(11.1%)	(10.6%)	(0.4%)

310 The uncorrected EKO AOD shows slopes  $\sim 1.06$  and correlation coefficients over 0.97 for all wavelengths. The RMS ranges from 0.017 (28.9%) at 340 nm to 0.004 (18.8%) at 870 nm. These results improve significantly when taking into account the CSR corrections for all wavelengths. Thus, for the corrected EKO AOD the correlation coefficients are  $\sim 0.98$  for the shorter wavelengths and  $\sim 1$  for the rest of the wavelengths. The RMS and MB show the same trend as that for the uncorrected EKO AOD case, that is, we find the lowest values for the higher wavelengths. The negative values of the MB (EKO AOD – Cimel AOD), indicate that the EKO AOD values are normally lower than the Cimel AOD values. However, these values are within the Cimel instrument uncertainties,  $\pm 0.01$  in the VIS and near-IR and  $\pm 0.02$  in the UV ranges (Eck et al., 1999). These results also agree with other studies. For example, Estellés et al. (2006) and Cachorro et al. (2009) found differences between 0.01 and 0.03 in the VIS range, and between 0.02 and 0.05 for the UV when comparing Li-cor AOD with Cimel AOD. Recently, Kazadzis et al. (2018a) found AOD differences ranging between 0.01 and 0.03 at 500 and 865 nm, respectively, when comparing AOD from PSR and PFR. Recently, Cuevas et al. (2019), using long-term AOD data series from both GAW-PFR and AERONET-320

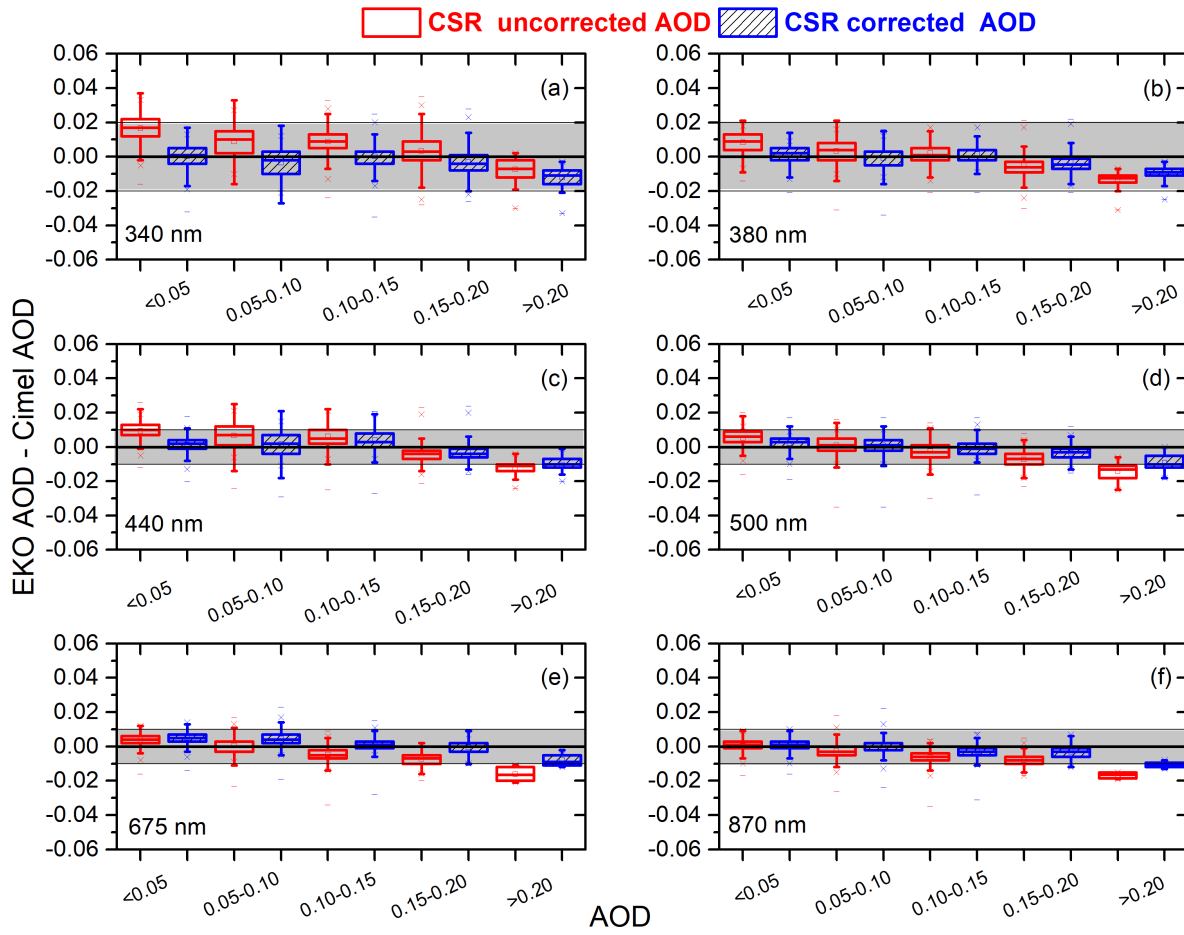


**Figure 10.** Box plot of the differences between the EKO AOD with (no) CSR corrections, and Cimel AOD versus AOD for the period April-September 2019 at IZO in blue (red). Lower and upper boundaries for each box are the 25<sup>th</sup> and 75<sup>th</sup> percentiles; the solid line is the median value; the crosses indicate values out of the 1.5-fold box area (outliers); and hyphens are the maximum and minimum values. Shadings show the range of uncertainty of Cimel ( $\pm 0.02$  for the UV range and  $\pm 0.01$  for VIS and near-IR ranges; Eck et al. (1999)).

Cimel radiometers reported differences in AOD  $\sim 3\%$  lower at 380 nm and  $\sim 2\%$  lower at 500 nm for GAW-PFR due to its larger FOV.

The box plots of MB differences (EKO AOD – Cimel AOD) for different AOD intervals are presented in Figure 10. In general, it can be seen that a significant improvement in the AOD retrievals is found after CSR correction, with the corrected AOD medians being closer to 0 in all wavelengths. The improvement in AOD for AOD>0.1 conditions is also remarkable (20% of the data for 340 and 380 nm, and 16% for the rest of the wavelengths) is remarkable, as already mentioned in the CSR correction section. The scatter also is significantly reduced for all wavelengths and aerosol loads, except in the 340 nm UV channel. This is mainly attributed to the higher instrument uncertainty, as well as

**Table 5.** Linear AOD-correction equations (slope and intercept) at 340, 380, 440, 500, 675 and 870 nm obtained with data measured from April 1st to July 31<sup>st</sup> 2019 at Izaña Observatory. Validation of the linear AOD-correction equations was performed using data obtained between August 1<sup>st</sup> and September 30<sup>th</sup> 2019.

Linear AOD-correction Equations:				Validation		
Corrected EKO AOD = Slope*EKO AOD + Intercept				01/08/2019-30/09/2019		
01/04/2019-31/07/2019						
Wavelength	Slope	Intercept	R	RMS	MB	R
(nm)						
<b>340</b>	1.076	-0.019	0.997	0.005 (5.9%)	-0.003 (-4.0%)	0.998
<b>380</b>	1.073	-0.0102	0.999	0.003 (2.9%)	-0.003 (-1.6%)	0.999
<b>440</b>	1.066	<0.001	0.999	0.002 (2.4%)	<0.001 (-1.2%)	0.999
<b>500</b>	1.056	-0.005	0.999	0.002 (2.9%)	-0.001 (-2.1%)	0.999
<b>675</b>	1.043	0.003	0.999	0.001 (2.4%)	<0.001 (-1.7%)	0.999
<b>870</b>	1.031	<0.001	0.999	<0.001 (1.4%)	<0.001 (-0.02%)	0.999

a poorer model aerosol characterization this range (see Sect. 2.2). Since the 340 nm instrumental error in the spectral range

330 between 300 and 380 nm channels have 350 nm (17.2%), of which 6% corresponds to stray-light and 6% corresponds to measurement repeatability (Zong et al., 2006), to the different FWHM between EKO (7 nm) and CIMEL (2 nm) at 340 nm, and 4 nm bandpass, respectively, and the EKO MS-711 FWHM is  $\sim$  7 nm (Table 1), these two UV channels have some additional radiation contribution from the adjacent wavelengths, increasing their uncertainty and causing an AOD overestimation to the fact that Rayleigh and aerosol scattering are higher in the UV range (Cuevas et al., 2019). Despite these drawbacks, the improvement in AOD is significant performing a simple correction of the CSR estimated with LibRadtran.

335 The linear AOD-correction equations were determined by using data measured from April 1<sup>st</sup> to July 31<sup>th</sup> 2019 (69% of the data) at Izaña Observatory (Table 5). The validation of these linear AOD-correction equations was performed using an independent period of data (between August 1<sup>st</sup> and September 30<sup>th</sup> 2019; 31% of the data). Note that  $MB \geq -1.6abs(MB) \leq 1.6\%$  for all wavelengths except for 340 nm for which a significantly larger MB (-4.0%) is registered. In any case it should be noted that the CSR correction applied in this study has been made under the presence of mineral dust. It would be necessary to verify that these CRS corrections have similar validity under moderate-high influence of other types of aerosols, such as marine or biomass burning aerosols.

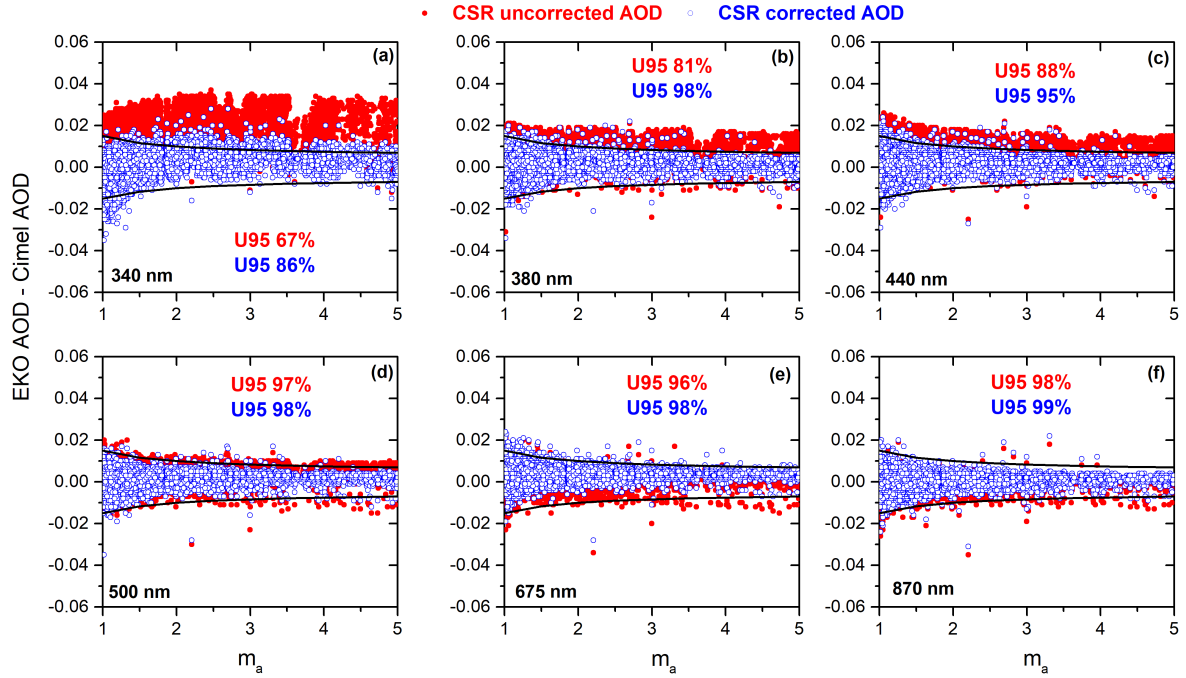


**Figure 11.** AOD differences (EKO AOD – Cimel AOD) versus the optical air mass ( $m_a$ ). Black lines represent the  $U_{95}$  uncertainty limits.

In order to check the quality of EKO AOD, we have applied the WMO traceability criteria (WMO, 2005) defined for finite FOV instruments as:

345  $U_{95} = \pm(0.005 + 0.010m_a)$  (21)

where  $m_a$  is the optical air mass. The percentage of data meeting the WMO traceability requirements (95% of the AOD differences of an instrument compared to the WMO standards lie within specific limits) is  $> 95\%$  at 500, 675 and 870 nm, taking the AERONET-Cimel as the reference (Figure 11).

The percentage of EKO AOD data meeting the WMO criteria increases considerably when we take into account the CSR 350 corrections, increasing from 67% to more than 86% at 340 nm, and above 95% for the rest of the channels. The poorest results shown by the 340 nm channel (86%), might be partially explained by the EKO's 7nm FWHM influence on the smaller 2 and 4nm band pass UV channels. The instrument uncertainty is larger in the UV range, which is mostly associated with stray-light in the instrument inner optics (Zong et al., 2006).

When focusing the analysis on relatively high AOD (AOD  $> 0.10$ ), we found that the percentage of AOD differences out 355 of the WMO  $U_{95}$  limits were  $\sim 3.5\%$  (0.8% of the data) at 380 nm and  $0.6\%$  (0.3% of the data) at 870 nm, consistent with the lower percentages of AOD differences out of the WMO  $U_{95}$  reported by Cuevas et al. (2019) when comparing GAW-PFR (FOV  $\sim 2.5^\circ$ ) and AERONET-Cimel radiometers that present a lower difference in FOV ( $1.2^\circ$ ).

## 5 Conclusions

In this work, we present the characterization of an EKO MS-711 spectroradiometer. The instrument has been calibrated at 360 Izaña Observatory using the Langley-Plot method between April and September 2019. This calibration has been compared with the lamp calibration performed at EKO Instruments factory in 2016, obtaining relative differences  $\leq 2.3\%$  and 3.1% in the VIS and near IR range, respectively. These results indicate a high spectral stability of the instrument in this 3-year time period (2016-2019).

The EKO MS-711 has been designed for spectral solar DNI measurements, and therefore it has a relatively high FOV 365 (5°), double the FOV recommended by WMO for AOD radiometers, and four times larger than the AERONET-Cimel FOV. This difference in FOV might lead to a significant difference in near forward scattering under relatively high aerosol content, resulting in a small, but significant, AOD underestimation, especially in the UV range.

However, the AOD retrievals from an EKO MS-711 spectral DNI measurements show a rather good agreement with those from an AERONET reference radiometer. The AOD comparison was held at Izaña Observatory between April and September 370 2019. Quality assessment of the EKO MS-711 AOD has been performed by comparing with coincident AOD from AERONET at 340, 380, 440, 500, 675 and 870 nm considering measurements of both instruments as close as 2 minutes between them, with a total of 14706 analyzed data-pairs. The skill scores of the AOD comparison are fairly good with a RMS of 0.013 (24.6%) at 340 and 380 nm, and 0.029 (19.5%) for longer wavelengths (440, 500, 675 and 870 nm), with AOD being underestimated by the EKO radiometer. The MB (EKO AOD – Cimel AOD) are 0.011 (19.7%) for 340 and 380 nm and 0.004 (10.6%) for 375 440, 500, 675 and 870 nm. These results improve considerably when we take into account the CSR corrections to EKO AOD because of the higher EKO FOV. The CSR differences between EKO and AERONET-Cimel were obtained using LibRadtran model. When comparing EKO AOD corrected values the RMS is reduced to 0.006 (14.9%) at 340 and 380 nm, and to 0.005 (11.1%) for longer wavelengths, while MB is reduced to <0.001 (1.3%) for 340 and 380 nm, and <0.001 (0.4%) for 500, 675 and 870 nm. These values are within the Cimel instrumental uncertainty ( $\pm 0.01$  in the VIS and near-IR, and  $\pm 0.02$  in the UV 380 ranges).

Following WMO recommendations we have analysed the percentage of EKO AOD – Cimel AOD differences within WMO  $U_{95}$  limits defined for finite FOV instruments, we found that with no CSR-corrections  $\geq 96\%$  of the AOD differences fell within the WMO  $U_{95}$  limits at 500, 675 and 870 nm. After applying the CSR-corrections, the percentage of AOD differences within the WMO  $U_{95}$  limits were  $>95\%$  for 380, 440, 500, 675 and 870 nm, while for 340 nm the percentage of AOD differences 385 within the WMO  $U_{95}$  increased only to a modest 86%. The known greater AOD uncertainty in the UV range along with stray-light problems not fully corrected in this instrument seem to be behind the poorer AOD agreement with AERONET-Cimel at 340 nm.

The EKO-MS711 has proven to be an instrument, which despite having been designed for solar radiation measurements, can provide high quality AOD measurements in the VIS and near-IR ranges with excellent results when compared with the 390 AERONET-Cimel reference radiometer, which, in turn has shown a very good AOD traceability with the WORCC AOD world reference.

*Data availability.* The Cimel-AERONET data from the Izaña station (“Izana”) are available from the AERONET website: <https://aeronet.gsfc.nasa.gov/> (last access: 14 November 2019). The EKO MS-711 data might be available upon request to EKO Instruments and Izana WMO CIMO Testbed.

395 *Author contributions.* RDG and EC designed the structure and methodology of the paper and wrote the main part of the manuscript. RDG computed all the calculations performed in the paper. AB discussed the modelling results and participated in the AOD retrieval and the Langley calibration analysis. VEC provided interesting ideas used in this paper, and advice based on her experience in spectroradiometry. RR performed the maintenance and daily checks of the EKO-MS711 spectroradiometer. MP provided detailed technical information and calibrations of the EKO-MS711 spectroradiometer. KH allowed that the EKO-MS711 used in this study could be evaluated in the WMO  
400 CIMO Izaña testbed taking care of all the associated logistics. All authors discussed the results and contributed to the final paper.

*Competing interests.* The authors declare that they have no conflict of interest.

*Acknowledgements.* This work has been developed within the framework of the activities of the World Meteorological Organization (WMO) Commission for Instruments and Methods of Observation (CIMO) Izaña test bed for aerosols and water vapor remote sensing instruments. The authors are grateful to EKO Instruments for its availability that the EKO-MS711 spectroradiometer has been tested and evaluated  
405 independently by the WMO CIMO Izaña testbed. The LibRadtran Radiative Transfer Model has been used to estimate the circumsolar radiation. AERONET Sun photometers at Izaña have been calibrated within the AERONET Europe TNA, supported by the European Union Horizon 2020 research and innovation program under grant agreement no. 654109 (ACTRIS-2). This research benefited from the results of the project funding by MINECO RTI2018-097864-B-I00. We also acknowledge our colleague Celia Milford for improving the English of the manuscript.

410 **Appendix A:**

Abbreviations

AEMET State Meteorological Agency of Spain

AERONET AErosol RObotic NETwork

AOD Aerosol Optical Depth

415 BapMon Background Atmospheric Pollution Monitoring Network

BSRN Baseline Surface Radiation Network

CIMO Commission for Instruments and Methods of Observation

CSR Circumsolar Radiation

DNI Direct Normal Irradiance

420 FOV Field of View

	<u>FTIR Fourier Transform Infrared Spectrometer</u>
	<u>FWHM Full Width at Half Maximum</u>
	<u>GAW-PFR Precision Filter Radiometer Network</u>
	<u>GNSS Global Navigation Satellite System</u>
425	<u>IARC Izaña Atmospheric Research Center</u>
	<u>IZO Izaña Observatory</u>
	<u>MB Mean Bias</u>
	<u>NDACC Network for the Detection of Atmospheric Composite Change</u>
	<u>NIST National Institute of Standards and Technology</u>
430	<u>NOAA National Oceanic and Atmospheric Administration</u>
	<u>OPAC Optical Properties of Aerosols and Clouds</u>
	<u>PSR Precision Solar Spectroradiometer</u>
	<u>RMS Root Mean Square</u>
	<u>SKYNET SKYradiometer NETwork</u>
435	<u>SURFRAD SURFace RADiation Budget Network</u>
	<u>SZA Solar Zenith Angle</u>
	<u>UV Ultraviolet Range</u>
	<u>VIS Visible Range</u>
	<u>WMO World Meteorological Organization</u>
440	<u>WORCC World OpticalDepth Research and Calibration Center</u>
	<u>WRC-PMOD World Radiation Center- Physical Meteorological Observatory</u>

## Appendix B:

Numerical values of the CR (%) simulations for SZA  $30^\circ$  at sea level for AOD values between 0 and 2, at 500 nm, for different types of aerosols for FOV of  $5^\circ$ .

AOD	Continental	Continental	Continental	Urban	Maritime	Maritime	Maritime	Desert
	Clean	Average	Pollution	CR (%)	Clean	Pollution	Tropical	
	CR (%)	CR (%)	CR (%)	CR (%)	CR (%)	CR (%)	CR (%)	CR (%)
0.1	0.3	0.2	0.1	0.1	0.6	0.5	0.6	0.6
0.2	0.5	0.4	0.3	0.3	1.3	1.0	1.2	1.3
0.3	0.7	0.6	0.4	0.4	1.9	1.5	1.9	1.9
0.4	1.0	0.8	0.6	0.5	2.5	2.0	2.5	2.5
0.5	1.3	1.0	0.7	0.7	3.2	2.5	3.1	3.1
0.6	1.5	1.2	0.9	0.8	3.8	3.1	3.7	3.8
0.7	1.8	1.4	1.0	0.9	4.5	3.6	4.4	4.4
0.8	2.0	1.6	1.2	1.1	5.1	4.1	5.0	5.0
0.9	2.3	1.8	1.3	1.2	5.8	4.6	5.7	5.7
1	2.6	2.0	1.5	1.3	6.5	5.2	6.3	6.3
1.1	2.9	2.2	1.7	1.5	7.1	5.7	7.0	7.0
1.2	3.2	2.4	1.8	1.6	7.8	6.3	7.6	7.6
1.3	3.5	2.7	2.0	1.8	8.5	6.8	8.3	8.3
1.4	3.8	2.9	2.2	2.0	9.2	7.4	9.0	8.9
1.5	4.1	3.2	2.4	2.1	9.9	8.0	9.7	9.6
1.6	4.4	3.4	2.6	2.3	10.6	8.5	10.4	10.3
1.7	4.7	3.7	2.8	2.4	11.4	9.1	11.1	10.9
1.8	5.1	3.9	3.0	2.6	12.1	9.7	11.8	11.6
1.9	5.4	4.2	3.2	2.8	12.8	10.3	12.5	12.3
2	5.8	4.5	3.4	3.0	13.6	10.9	13.2	13.0

## References

Ahern, F. J., Gauthier, R. P., Teillet, P. M., Sirois, J., Fedosejevs, G., and Lorente, D.: Investigation of continental aerosols with high-spectral-resolution solar-extinction measurements, *Appl. Opt.*, 30, 5276–5287, <https://doi.org/10.1364/AO.30.005276>, 1991.

Anderson, G., Clough, S., Kneizys, F., Chetwynd, J., and Shettle, E.: AFGL atmospheric constituent profiles, *Environ. Res. Pap.*, 954, 1–46, 450 1986.

Ångström, A.: On the atmospheric transmission of sun radiation. II, *Geografiska Annaler*, 12, 130–159, 1930.

Ångström, A.: Techniques of determining the turbidity of the atmosphere, *Tellus*, 13, 214–223, 1961.

Ångström, A.: Apparent solar constant variations and their relation to the variability of atmospheric transmission, *Tellus*, 22, 205–218, <https://doi.org/https://doi.org/10.1111/j.2153-3490.1970.tb01522.x>, 1970.

Augustine, J. A., Hodges, G. B., Dutton, E. G., Michalsky, J. J., and Cornwall, C. R.: An aerosol optical depth climatology for NOAA's national surface radiation budget network (SURFRAD), *Journal of Geophysical Research: Atmospheres*, 113, 455 <https://doi.org/10.1029/2007JD009504>, 2008.

- Barreto, A., Cuevas, E., Pallé, P., Romero, P. M., Guirado, C., Wehrli, C. J., and Almansa, F.: Recovering long-term aerosol optical depth series (1976-2012) from an astronomical potassium-based resonance scattering spectrometer, *Atmospheric Measurement Techniques*, 7, 4103–4116, <https://doi.org/10.5194/amt-7-4103-2014>, 2014.
- 460
- Berjón, A., Barreto, A., Hernández, Y., Yela, M., Toledano, C., and Cuevas, E.: A 10-year characterization of the Saharan Air Layer lidar ratio in the subtropical North Atlantic, *Atmospheric Chemistry and Physics*, 19, 6331–6349, <https://doi.org/10.5194/acp-19-6331-2019>, <https://www.atmos-chem-phys.net/19/6331/2019/>, 2019.
- Berk, A., Acharya, P. K., Bernstein, L. S., Anderson, G. P., Chetwynd Jr, J. H., and Hoke, M. L.: Reformulation of the MODTRAN band model for higher spectral resolution, in: *Algorithms for Multispectral, Hyperspectral, and Ultraspectral Imagery VI*, vol. 4049, pp. 190–198, International Society for Optics and Photonics, <https://doi.org/https://doi.org/10.1117/12.410340>, 2000.
- 465
- Blanc, P., Espinar, B., Geuder, N., Gueymard, C., Meyer, R., Pitz-Paal, R., Reinhardt, B., Renné, D., Sengupta, M., Wald, L., and Wilbert, S.: Direct normal irradiance related definitions and applications: The circumsolar issue, *Solar Energy*, 110, 561 – 577, <https://doi.org/https://doi.org/10.1016/j.solener.2014.10.001>, 2014.
- 470
- Bodhaine, B. A., Wood, N. B., Dutton, E. G., and Slusser, J. R.: On Rayleigh optical depth calculations, *Journal of Atmospheric and Oceanic Technology*, 16, 1854–1861, 1999.
- Brion, J., Chakir, A., Daumont, D., Malicet, J., and Parisse, C.: High-resolution laboratory absorption cross section of O3. Temperature effect, *Chemical physics letters*, 213, 610–612, 1993.
- 475
- Brion, J., Chakir, A., Charbonnier, J., Daumont, D., Parisse, C., and Malicet, J.: Absorption spectra measurements for the ozone molecule in the 350–830 nm region, *Journal of atmospheric chemistry*, 30, 291–299, 1998.
- Burrows, J., Richter, A., Dehn, A., Deters, B., Himmelmann, S., Voigt, S., and Orphal, J.: Atmospheric remote-sensing reference data from GOME-2 temperature-dependent absorption cross sections of O3 in the 231–794 nm range, *Journal of Quantitative Spectroscopy and Radiative Transfer*, 61, 509–517, [https://doi.org/https://doi.org/10.1016/S0022-4073\(98\)00037-5](https://doi.org/https://doi.org/10.1016/S0022-4073(98)00037-5), 1999.
- Cachorro, V., Casanova, J., and de Frutos, A.: The influence of Angstrom parameters on calculated direct solar spectral irradiances at high 480 turbidity, *Solar Energy*, 39, 399 – 407, [https://doi.org/https://doi.org/10.1016/S0038-092X\(87\)80058-0](https://doi.org/https://doi.org/10.1016/S0038-092X(87)80058-0), 1987.
- Cachorro, V., Durán, P., and De Frutos, A.: Retrieval of vertical ozone content using the Chappuis band with high spectral resolution solar radiation measurements, *Geophysical research letters*, 23, 3325–3328, <https://doi.org/https://doi.org/10.1029/96GL03239>, 1996.
- Cachorro, V. E., Durán, P., Vergaz, R., and de Frutos, A. M.: Measurements of the atmospheric turbidity of the north-centre continental area in Spain: Spectral aerosol optical depth and Ångström turbidity parameters, *Journal of Aerosol Science*, 31, 687–702, 485 [https://doi.org/https://doi.org/10.1016/S0021-8502\(99\)00552-2](https://doi.org/https://doi.org/10.1016/S0021-8502(99)00552-2), 2000.
- Cachorro, V. E., Berjón, A., Toledano, C., Mogo, S., Prats, N., de Frutos, A. M., Vilaplana, J. M., Sorribas, M., De La Morena, B. A., Gröbner, J., and Laulainen, N.: Detailed Aerosol Optical Depth Intercomparison between Brewer and Li-Cor 1800 Spectroradiometers and a Cimel Sun Photometer, *Journal of Atmospheric and Oceanic Technology*, 26, 1558–1571, <https://doi.org/10.1175/2009JTECHA1217.1>, 2009.
- Cuevas, E., Milford, C., Bustos, J. J., del Campo-Hernández, García, O., D., G. R., Gómez-Peláez, Guirado-Fuentes, C., Marrero, C., Prats, 490 N., Ramos, R., Redondas, A., Reyes, E., Rodríguez, S., Romero-Campos, P., Scheneider, M., Belmonte, J., Yela, M., Almansa, F., Barreto, A., López-Solano, C., Basart, S., Terradellas, E., Afonso, S., Bayo, C., Berjón, A., Bethencourt, J., Carreño, V., Castro, N. J., Cruz, A. M., Damas, M., De Ory-Ajamil, F., García, M. I., Gómez-Trueba, V., González, Y., Hernández, C., Hernández, Y., Hernández-Cruz, B., Jover, M., León, S., López-Fernández, R., López-Solano, J., Rodríguez, E., Rodríguez-Franco, J., Rodríguez-Valido, M., Sálamo, C., Sanromá, E., Santana, D., Santo-Tomás, F., Sepúlveda, E., Sierra, M., and Sosa, E.: Izaña Atmospheric Research Center Activity Report 2015-2016, 495 State Meteorological Agency (AEMET), 2017.

- Cuevas, E., Romero-Campos, P. M., Kouremeti, N., Kazadzis, S., Räisänen, P., García, R. D., Barreto, A., Guirado-Fuentes, C., Ramos, R., Toledano, C., Almansa, F., and Gröbner, J.: Aerosol optical depth comparison between GAW-PFR and AERONET-Cimel radiometers from long-term (2005–2015) 1 min synchronous measurements, *Atmospheric Measurement Techniques*, 12, 4309–4337, <https://doi.org/10.5194/amt-12-4309-2019>, <https://www.atmos-meas-tech.net/12/4309/2019/>, 2019.
- 500 500 Eck, T., Holben, B., Reid, J., Dubovik, O., Smirnov, A., O’neill, N., Slutsker, I., and Kinne, S.: Wavelength dependence of the optical depth of biomass burning, urban, and desert dust aerosols, *Journal of Geophysical Research: Atmospheres*, 104, 31 333–31 349, <https://doi.org/10.1029/1999JD900923>, 1999.
- Egli, L., Gröbner, J., Hülsen, G., Bachmann, L., Blumthaler, M., Dubard, J., Khazova, M., Kift, R., Hoogendijk, K., Serrano, A., Smedley, A., and Vilaplana, J.-M.: Quality assessment of solar UV irradiance measured with 505 array spectroradiometers, *Atmospheric Measurement Techniques*, 9, 1553–1567, <https://doi.org/10.5194/amt-9-1553-2016>, <https://www.atmos-meas-tech.net/9/1553/2016/>, 2016.
- Emde, C., Buras-Schnell, R., Kylling, A., Mayer, B., Gasteiger, J., Hamann, U., Kylling, J., Richter, B., Pause, C., Dowling, T., et al.: The libRadtran software package for radiative transfer calculations (version 2.0. 1), *Geoscientific Model Development*, pp. 1647–1672, <https://doi.org/http://doi.org/10.5194/gmd-9-1647-2016>, 2016.
- 510 510 Emilio, M., Kuhn, J. R., Bush, R. I., and Scholl, I. F.: Measuring the solar radius from space during the 2003 and 2006 mercury transits, *The Astrophysical Journal*, 750, <https://doi.org/10.1088/0004-637x/750/2/135>, 2012.
- Estellés, V., Utrillas, M., Martínez-Lozano, J., Alcántara, A., Alados-Arboledas, L., Olmo, F., Lorente, J., De Cabo, X., Cachorro, V., Horvath, H., et al.: Intercomparison of spectroradiometers and Sun photometers for the determination of the aerosol optical depth during the VELETA-2002 field campaign, *Journal of Geophysical Research: Atmospheres*, 111, <https://doi.org/https://doi.org/10.1029/2005JD006047>, 2006.
- 515 515 García, M. I., Rodríguez, S., and Alastuey, A.: Impact of North America on the aerosol composition in the North Atlantic free troposphere, *Atmospheric Chemistry and Physics*, 17, 7387–7404, <https://doi.org/10.5194/acp-17-7387-2017>, <https://www.atmos-chem-phys.net/17/7387/2017/>, 2017.
- García, R. D., García, O. E., Cuevas, E., Cachorro, V. E., Romero-Campos, P. M., Ramos, R., and de Frutos, A. M.: Solar radiation measurements compared to simulations at the BSRN Izaña station. Mineral dust radiative forcing and efficiency study, *Journal of Geophysical Research: Atmospheres*, 119, 179–194, <https://doi.org/doi:10.1002/2013JD020301>, 2014.
- 520 520 Gasteiger, J., Emde, C., Mayer, B., Buras, R., Buehler, S., and Lemke, O.: Representative wavelengths absorption parameterization applied to satellite channels and spectral bands, *Journal of Quantitative Spectroscopy and Radiative Transfer*, 148, 99–115, <https://doi.org/http://dx.doi.org/10.1016/j.jqsrt.2014.06.024>, 2014.
- Giles, D. M., Sinyuk, A., Sorokin, M. G., Schafer, J. S., Smirnov, A., Slutsker, I., Eck, T. F., Holben, B. N., Lewis, J. R., Campbell, J. R., Welton, E. J., Korkin, S. V., and Lyapustin, A. I.: Advancements in the Aerosol Robotic Network (AERONET) Version 3 database – automated near-real-time quality control algorithm with improved cloud screening for Sun photometer aerosol optical depth (AOD) measurements, *Atmospheric Measurement Techniques*, 12, 169–209, <https://doi.org/10.5194/amt-12-169-2019>, <https://www.atmos-meas-tech.net/12/169/2019/>, 2019.
- 530 530 Gröbner, J., Vergaz, R., Cachorro, V. E., Henriques, D., Lamb, K., Redondas, A., Vilaplana, J. M., and Rembges, D.: Intercomparison of aerosol optical depth measurements in the UVB using Brewer Spectrophotometers and a Li-Cor Spectrophotometer, *Geophysical research letters*, 28, 1691–1694, <https://doi.org/https://doi.org/10.1029/2000GL012759>, 2001.

- Guemard, C.: SMARTS2: a simple model of the atmospheric radiative transfer of sunshine: algorithms and performance assessment, Florida Solar Energy Center Cocoa, FL, 1995.
- 535 Guemard, C. A.: Parameterized transmittance model for direct beam and circumsolar spectral irradiance, *Solar Energy*, 71, 325–346, [https://doi.org/https://doi.org/10.1016/S0038-092X\(01\)00054-8](https://doi.org/https://doi.org/10.1016/S0038-092X(01)00054-8), 2001.
- Halthore, R. N., Schwartz, S. E., Michalsky, J. J., Anderson, G. P., Ferrare, R. A., Holben, B. N., and Ten Brink, H. M.: Comparison of model estimated and measured direct-normal solar irradiance, *Journal of Geophysical Research: Atmospheres*, 102, 29 991–30 002, <https://doi.org/10.1029/97JD02628>, 1997.
- 540 Hansen, J. E. and Travis, L. D.: Light scattering in planetary atmospheres, *Space science reviews*, 16, 527–610, <https://doi.org/https://doi.org/10.1007/BF00168069>, 1974.
- Hess, M., Koepke, P., and Schult, I.: Optical properties of aerosols and clouds: The software package OPAC, *Bulletin of the American meteorological society*, 79, 831–844, [https://doi.org/https://doi.org/10.1175/1520-0477\(1998\)079<0831:OPOAAC>2.0.CO;2](https://doi.org/https://doi.org/10.1175/1520-0477(1998)079<0831:OPOAAC>2.0.CO;2), 1998.
- Holben, B., Eck, T., Slutsker, I., Tanré, D., Buis, J., Setzer, A., Vermote, E., Reagan, J., Kaufman, Y., Nakajima, T., Lavenu, F., Jankowiak, 545 I., and Smirnov, A.: AERONET—A Federated Instrument Network and Data Archive for Aerosol Characterization, *Remote Sensing of Environment*, 66, 1 – 16, [https://doi.org/https://doi.org/10.1016/S0034-4257\(98\)00031-5](https://doi.org/https://doi.org/10.1016/S0034-4257(98)00031-5), 1998.
- Holben, B., Tanre, D., Smirnov, A., Eck, T., Slutsker, I., Abu Hassan, N., Newcomb, W., Schafer, J., Chatenet, B., Lavenu, F., et al.: An emerging ground-based aerosol climatology: Aerosol optical depth from AERONET, *Journal of Geophysical Research: Atmospheres*, 106, 12 067–12 097, <https://doi.org/https://doi.org/10.1029/2001JD900014>, 2001.
- 550 IPCC: The Physical Science Basis. Intergovernmental Panel on Climate Change, <https://doi.org/doi:10.1017/CBO9781107415324>, 2013.
- Kasten, F.: A new table and approximation formula for the relative optical air mass, *Arch. Meteor. Geophy. B*, 14, 206–223, 1966.
- Kasten, F. and Young, A. T.: Revised optical air mass tables and approximation formula, *Appl. Opt.*, 28, 4735–4738, <https://doi.org/10.1364/AO.28.004735>, 1989.
- Kazadzis, S., Bais, A., Kouremeti, N., Gerasopoulos, E., Garane, K., Blumthaler, M., Schallhart, B., and Cede, A.: Direct spectral 555 measurements with a Brewer spectroradiometer: absolute calibration and aerosol optical depth retrieval, *Appl. Opt.*, 44, 1681–1690, <https://doi.org/10.1364/AO.44.001681>, 2005.
- Kazadzis, S., Veselovskii, I., Amiridis, V., Gröbner, J., Suvorina, A., Nyeki, S., Gerasopoulos, E., Kouremeti, N., Taylor, M., Tsekeli, A., and Wehrli, C.: Aerosol microphysical retrievals from precision filter radiometer direct solar radiation measurements and comparison with AERONET, *Atmospheric Measurement Techniques*, 7, 2013–2025, <https://doi.org/10.5194/amt-7-2013-2014>, <http://www.atmos-meas-tech.net/7/2013/2014/>, 2014.
- Kazadzis, S., Kouremeti, N., Diémoz, H., Gröbner, J., Forgan, B. W., Campanelli, M., Estellés, V., Lantz, K., Michalsky, J., Carlund, T., Cuevas, E., Toledano, C., Becker, R., Nyeki, S., Kosmopoulos, P. G., Tatsiankou, V., Vuilleumier, L., Denn, F. M., Ohkawara, N., Ijima, O., Goloub, P., Raptis, P. I., Milner, M., Behrens, K., Barreto, A., Martucci, G., Hall, E., Wendell, J., Fabbri, B. E., and Wehrli, C.: Results from the Fourth WMO Filter Radiometer Comparison for aerosol optical depth measurements, *Atmospheric Chemistry and Physics*, 18, 560 3185–3201, <https://doi.org/10.5194/acp-18-3185-2018>, 2018a.
- Kazadzis, S., Kouremeti, N., Nyeki, S., Gröbner, J., and Wehrli, C.: The World Optical Depth Research and Calibration Center (WORCC) quality assurance and quality control of GAW-PFR AOD measurements, *Geoscientific Instrumentation, Methods and Data Systems*, 7, 39–53, <https://doi.org/10.5194/gi-7-39-2018>, 2018b.

- 570 Kiedron, P. W. and Michalsky, J. J.: Non-parametric and least squares Langley plot methods, *Atmospheric Measurement Techniques*, 9, 215–225, <https://doi.org/10.5194/amt-9-215-2016>, <https://www.atmos-meas-tech.net/9/215/2016/>, 2016.
- Komhyr, W. D., Grass, R. D., and Leonard, R. K.: Dobson spectrophotometer 83: A standard for total ozone measurements, 1962–1987, *Journal of Geophysical Research: Atmospheres*, 94, 9847–9861, 1989.
- Kurucz, R. L.: Synthetic infrared spectra, in: *Infrared solar physics*, pp. 523–531, Springer, 1994.
- 575 López-Solano, J., Redondas, A., Carlund, T., Rodriguez-Franco, J. J., Diémoz, H., León-Luis, S. F., Hernández-Cruz, B., Guirado-Fuentes, C., Kouremeti, N., Gröbner, J., Kazadzis, S., Carreño, V., Berjón, A., Santana-Díaz, D., Rodríguez-Valido, M., De Bock, V., Moreta, J. R., Rimmer, J., Smedley, A. R. D., Boulkelia, L., Jepsen, N., Eriksen, P., Bais, A. F., Shiroto, V., Vilaplana, J. M., Wilson, K. M., and Karppinen, T.: Aerosol optical depth in the European Brewer Network, *Atmospheric Chemistry and Physics*, 18, 3885–3902, <https://doi.org/10.5194/acp-18-3885-2018>, <https://www.atmos-chem-phys.net/18/3885/2018/>, 2018.
- 580 Major, G.: A method for determining the circumsolar sky function, *Tellus*, 32, 340–347, <https://doi.org/https://doi.org/10.1111/j.2153-3490.1980.tb00961.x>, 1980.
- Mayer, B.: Radiative transfer in the cloudy atmosphere, in: *EPJ Web of Conferences*, vol. 1, pp. 75–99, EDP Sciences, <https://doi.org/https://doi.org/10.1140/epjconf/e2009-00912-1>, 2009.
- Mayer, B. and Kylling, A.: Technical note: The libRadtran software package for radiative transfer calculations - description and examples of 585 use, *Atmospheric Chemistry and Physics*, 5, 1855–1877, <https://doi.org/10.5194/acp-5-1855-2005>, <https://www.atmos-chem-phys.net/5/1855/2005/>, 2005.
- Michalsky, J., Liljegren, J., and Harrison, L.: A comparison of sun photometer derivations of total column water vapor and ozone to standard measures of same at the Southern Great Plains Atmospheric Radiation Measurement site, *Journal of Geophysical Research: Atmospheres*, 100, 25 995–26 003, <https://doi.org/https://doi.org/10.1029/95JD02706>, 1995.
- 590 Neumann, A. and Witzke, A.: The influence of sunshape on the DLR solar furnace beam, *Solar Energy*, 66, 447–457, [https://doi.org/https://doi.org/10.1016/S0038-092X\(99\)00048-1](https://doi.org/https://doi.org/10.1016/S0038-092X(99)00048-1), 1999.
- Pastiels, R.: Contribution à l'étude du problème des méthodes actinométriques, 1959.
- Pierluissi, J. H. and Tsai, C.-M.: Molecular transmittance band model for oxygen in the visible, *Applied optics*, 25, 2458–2460, <https://doi.org/https://doi.org/10.1364/AO.25.002458>, 1986.
- 595 Pierluissi, J. H. and Tsai, C.-M.: New LOWTRAN models for the uniformly mixed gases, *Applied optics*, 26, 616–618, <https://doi.org/https://doi.org/10.1364/AO.26.000616>, 1987.
- Pó, M., Hoogendijk, K., Beuttell, W., Kazunori, S., and Takeuchi, E.: Direct Spectral Irradiance Measurements from Rotating Shadowband EKO Grating Spectroradiometer, in: *2018 IEEE 7th World Conference on Photovoltaic Energy Conversion (WCPEC)(A Joint Conference of 45th IEEE PVSC, 28th PVSEC & 34th EU PVSEC)*, pp. 2337–2340, IEEE, <https://doi.org/10.1109/PVSC.2018.8547445>, 2018.
- 600 Räisänen, P. and Lindfors, A. V.: On the Computation of Apparent Direct Solar Radiation, *Journal of the Atmospheric Sciences*, 76, 2761–2780, <https://doi.org/10.1175/JAS-D-19-0030.1>, 2019.
- Raptis, P.-I., Kazadzis, S., Gröbner, J., Kouremeti, N., Doppler, L., Becker, R., and Helmis, C.: Water vapour retrieval using the Precision Solar Spectroradiometer, *Atmospheric Measurement Techniques*, 11, 1143–1157, <https://doi.org/10.5194/amt-11-1143-2018>, <https://www.atmos-meas-tech.net/11/1143/2018/>, 2018.
- 605 Redondas, A., Nevas, S., Berjón, A., Sildoja, M.-M., León-Luis, S. F., Carreño, V., and Santana-Díaz, D.: Wavelength calibration of Brewer spectrophotometer using a tunable pulsed laser and implications to the Brewer ozone retrieval, *Atmospheric Measurement Techniques*, 11, 3759–3768, <https://doi.org/10.5194/amt-11-3759-2018>, <https://www.atmos-meas-tech.net/11/3759/2018/>, 2018.

Reinhardt, B.: On the retrieval of circumsolar radiation from satellite observations and weather model output, Ph.D. thesis, LMU München: Faculty of Physics, 2013.

- 610 Romero Campos, P. M., Cuevas Agulló, E., Ramos López, R., Valdés Pérez de Vargas, M., and Schneider, M.: Programa de vapor de agua en columna del Centro de Investigación Atmosférica de Izaña: Análisis e Intercomparación de diferentes Técnicas de Medida, NIPO 784-09-009-9, Agencia Estatal de Meteorología, Ministerio de Medio Ambiente, y Medio Rural y Marino, 2009.
- 615 Rothman, L., Gordon, I., Babikov, Y., Barbe, A., Benner, D. C., Bernath, P., Birk, M., Bizzocchi, L., Boudon, V., Brown, L., Campargue, A., Chance, K., Cohen, E., Coudert, L., Devi, V., Drouin, B., Fayt, A., Flaud, J.-M., Gamache, R., Harrison, J., Hartmann, J.-M., Hill, C., Hodges, J., Jacquemart, D., Jolly, A., Lamouroux, J., Roy, R. L., Li, G., Long, D., Lyulin, O., Mackie, C., Massie, S., Mikhailenko, S., Müller, H., Naumenko, O., Nikitin, A., Orphal, J., Perevalov, V., Perrin, A., Polovtseva, E., Richard, C., Smith, M., Starikova, E., Sung, K., Tashkun, S., Tennyson, J., Toon, G., Tyuterev, V., and Wagner, G.: The HITRAN2012 molecular spectroscopic database, *Journal of Quantitative Spectroscopy and Radiative Transfer*, 130, 4–50, [https://doi.org/https://doi.org/10.1016/j.jqsrt.2013.07.002](https://doi.org/10.1016/j.jqsrt.2013.07.002), 2013.
- 620 Schmid, B., Michalsky, J., Halthore, R., Beauharnois, M., Harrison, L., Livingston, J., Russell, P., Holben, B., Eck, T., and Smirnov, A.: Comparison of aerosol optical depth from four solar radiometers during the fall 1997 ARM intensive observation period, *Geophysical Research Letters*, 26, 2725–2728, <https://doi.org/10.1029/1999GL900513>, <https://agupubs.onlinelibrary.wiley.com/doi/abs/10.1029/1999GL900513>, 1999.
- 625 Schmid, B., Michalsky, J., Slater, D., Barnard, J., Halthore, R., Liljegren, J., Holben, B., Eck, T., Livingston, J., Russell, Philip B.R., I. T., and I., S.: Comparison of columnar water-vapor measurements from solar transmittance methods, *Applied Optics*, 40, 1886–1896, <https://doi.org/https://doi.org/10.1364/AO.40.001886>, 2001.
- Schneider, M., Blumenstock, T., Chipperfield, M. P., Hase, F., Kouker, W., Reddmann, T., Ruhnke, R., Cuevas, E., and Fischer, H.: Subtropical trace gas profiles determined by ground-based FTIR spectroscopy at Iza241;a (28deg; N, 16deg; W): Five-year record, error analysis, and comparison with 3-D CTMs, *Atmospheric Chemistry and Physics*, 5, 153–167, <https://doi.org/10.5194/acp-5-153-2005>, <https://www.atmos-chem-phys.net/5/153/2005/>, 2005.
- 630 Sengupta, M., Habte, A. M., Xie, Y., Lopez, A. J., Dooraghi, M., Kutchenreiter, M. C., Andreas, A. M., Reda, I. M., Maclaurin, G. J., Foster, M. J., and Gueymard, C.: Solar Resource Calibration, Measurement, and Dissemination: Final Report FY 2016-FY 2018, Tech. rep., National Renewable Energy Lab.(NREL), Golden, CO (United States), <https://doi.org/10.2172/1513198>, 2019.
- Shaw, G. E.: Sun Photometry, *Bulletin of the American Meteorological Society*, 64, 4–10, [https://doi.org/10.1175/1520-0477\(1983\)064<0004:SP>2.0.CO;2](https://doi.org/10.1175/1520-0477(1983)064<0004:SP>2.0.CO;2), 1983.
- 635 Shaw, G. E., Reagan, J. A., and Herman, B. M.: Investigations of atmospheric extinction using direct solar radiation measurements made with a multiple wavelength radiometer, *Journal of Applied Meteorology*, 12, 374–380, [https://doi.org/10.1175/1520-0450\(1973\)012<0374:IAEUD>2.0.CO;2](https://doi.org/10.1175/1520-0450(1973)012<0374:IAEUD>2.0.CO;2), 1973.
- Sinyuk, A., Holben, B. N., Smirnov, A., Eck, T. F., Slutsker, I., Schafer, J. S., Giles, D. M., and Sorokin, M.: Assessment of error in aerosol optical depth measured by AERONET due to aerosol forward scattering, *Geophysical Research Letters*, 39, <https://doi.org/10.1029/2012GL053894>, 2012.
- 640 Stamnes, K., Tsay, S.-C., Wiscombe, W., and Jayaweera, K.: Numerically stable algorithm for discrete-ordinate-method radiative transfer in multiple scattering and emitting layered media, *Applied optics*, 27, 2502–2509, <https://doi.org/https://doi.org/10.1364/AO.27.002502>, 1988.

- Stamnes, K., Tsay, S.-C., Wiscombe, W., and Laszlo, I.: DISORT, a general-purpose Fortran program for discrete-ordinate-method radiative  
645 transfer in scattering and emitting layered media: documentation of methodology, Tech. rep., Tech. rep., Dept. of Physics and Engineering  
Physics, Stevens Institute of Technology, Hoboken, NJ 07030, 2000.
- Takamura, T. and Nakajima, T.: Overview of SKYNET and its activities, *Optica pura y aplicada*, 37, 3303–3308, 2004.
- Toledano, C., González, R., Fuertes, D., Cuevas, E., Eck, T. F., Kazadzis, S., Kouremeti, N., Gröbner, J., Goloub, P., Blarel, L., Román, R.,  
650 Barreto, A., Berjón, A., Holben, B. N., and Cachorro, V. E.: Assessment of Sun photometer Langley calibration at the high-elevation sites  
Mauna Loa and Izaña, *Atmospheric Chemistry and Physics*, 18, 14 555–14 567, <https://doi.org/10.5194/acp-18-14555-2018>, 2018.
- Vergaz, R., Cachorro, V. E., De Frutos, M., Vilaplana, J. M., and De La Morena, B. A.: Columnar characteristics of aerosols by spec-  
troradiometer measurements in the maritime area of the Cadiz Gulf (Spain), *International Journal of Climatology*, 25, 1781–1804,  
655 <https://doi.org/10.1002/joc.1208>, 2005.
- Wehrli, C.: Calibrations of filter radiometers for determination of atmospheric optical depth, *Metrologia*, 37, 419, <http://stacks.iop.org/0026-1394/37/i=5/a=16>, 2000.
- Wehrli, C.: GAWPFR: A network of aerosol optical depth observations with precision filter radiometers, *GLOBAL ATMOSPHERE WATCH*,  
p. 36, 2005.
- Wehrli, C.: Precision Filter Radiometer Documentation, Version 4.0, 38 pp., Davos Dorf, 2008.
- WMO: Recent progress in sunphotometry: determination of the aerosol optical depth, WMO/TD-No. 143; GAW Report-No. 43, 1986.
- 660 WMO: WMO/GAW Experts Workshop on a Global Surface-Based Network for Long Term Observations of Column Aerosol Optical Prop-  
erties, GAW Report No. 162, WMO TD No. 1287, [https://library.wmo.int/pmb\\_ged/wmo-td\\_1287.pdf](https://library.wmo.int/pmb_ged/wmo-td_1287.pdf), 2005.
- WMO: Fourth WMO Workshop on the Impact of Various Observing Systems on Numerical Weather Prediction WMO/TD No. 1450,  
World Weather Watch, [https://www.wmo.int/pages/prog/www/OSY/Meetings/NWP-4-Geneva2008/Abridged\\_Version.pdf](https://www.wmo.int/pages/prog/www/OSY/Meetings/NWP-4-Geneva2008/Abridged_Version.pdf)(lastaccess:  
14November2019), 2008.
- 665 WMO: Commission for Instruments and Methods of Observation, Sixteenth session WMO no.1138, Saint Petersburg, Secretariat of the World  
Meteorological Organization, 2014.
- WMO: WMO/GAW Aerosol Measurement Procedures, Guidelines and Recommendations, 2nd Edition, WMO-No. 1177; GAW Report-No.  
670 227, Guidelines and Recommendations, [https://library.wmo.int/doc\\_num.php?explnum\\_id=3073](https://library.wmo.int/doc_num.php?explnum_id=3073), 2016.
- Yoon, H. W., Sperfeld, P., Yousef, S. G., and Metzdorf, J.: NIST-PTB measurements of the radiometric temperatures of a high-temperature  
black body using filter radiometers, *Metrologia*, 37, 377, <https://doi.org/10.1088/0026-1394/37/5/7>, 2000.
- Zong, Y., Brown, S. W., Johnson, B. C., Lykke, K. R., and Ohno, Y.: Simple spectral stray light correction method for array spectroradiome-  
ters, *Appl. Opt.*, 45, 1111–1119, <https://doi.org/10.1364/AO.45.001111>, <http://ao.osa.org/abstract.cfm?URI=ao-45-6-1111>, 2006.